

# A Bayesian analysis of sneutrino DM in the NMSSM with Type-I seesaw mechanism

---

Junjie Cao<sup>1,2</sup>, Xiaofei Guo<sup>1</sup>, Yusi Pan<sup>1</sup>, Liangliang Shang<sup>1</sup>, Yuanfang Yue<sup>1</sup>

<sup>1</sup> *College of Physics and Materials Science, Henan Normal University, Xinxiang 453007, China*

<sup>2</sup> *Center for High Energy Physics, Peking University, Beijing 100871, China*

*E-mail:* [junjiec@itp.ac.cn](mailto:junjiec@itp.ac.cn), [guoxf@gs.zzu.edu.cn](mailto:guoxf@gs.zzu.edu.cn),  
[panyusi0406@foxmail.com](mailto:panyusi0406@foxmail.com), [shlwell1988@gmail.com](mailto:shlwell1988@gmail.com), [yuanfang405@gmail.com](mailto:yuanfang405@gmail.com)

ABSTRACT: In the Next-to-Minimal Supersymmetric Standard Model (NMSSM) with extra heavy neutrino superfields, neutrino can acquire its mass via a seesaw mechanism and sneutrino may act as a viable dark matter (DM) candidate. Given the strong tension between the naturalness for  $Z$  boson mass and the DM direct detection experiments for customary neutralino DM candidate, we augment the NMSSM with Type-I seesaw mechanism, which is the simplest extension of the theory to predict neutrino mass, and study the scenarios of sneutrino DM. We construct likelihood function with B-physics measurements, LHC Higgs data, DM relic density and its direct and indirect search limits, and perform a comprehensive scan over the parameter space of the theory by Nested Sampling method. We adopt both Bayesian and frequentist statistical quantities to illustrate the favored parameter space of the scenarios, the DM annihilation mechanism as well as the features of DM-nucleon scattering. We find that the scenarios are viable over broad parameter regions, and the DM usually co-annihilated with the Higgsinos to get the measured relic density. Interestingly, our results indicate that a rather low Higgsino mass,  $\mu \lesssim 250\text{GeV}$ , is preferred in the scan, and the DM-nucleon scattering rate is naturally suppressed to coincide with the recent XENON-1T results. Other issues, such as the LHC search for the Higgsinos, are also addressed.

---

## Contents

<b>1</b>	<b>Introduction</b>	<b>2</b>
<b>2</b>	<b>NMSSM with Type-I Mechanism</b>	<b>4</b>
2.1	Model Lagrangian	5
2.2	Sneutrino mass	6
2.3	DM Relic density	7
2.4	DM Direct detection	8
<b>3</b>	<b>Numerical Results</b>	<b>10</b>
3.1	Scan strategy	10
3.2	Favored parameter regions	13
3.3	DM annihilation mechanisms	14
3.4	DM-nucleon scattering	16
<b>4</b>	<b>Constraints from the LHC experiments</b>	<b>17</b>
<b>5</b>	<b>Conclusions</b>	<b>18</b>

---

## 1 Introduction

A large number of cosmological and astrophysical observations have firmly established the existence of non-baryonic DM [1–4]. Among the possible candidates, the weakly interactive massive particles (WIMPs) are most attractive since they naturally lead to right DM abundance [5, 6]. So far this type of DM candidates are still compatible with the more and more stringent constraints from DM direct and indirect search experiments, which was recently emphasized in [7]. As the most popular ultraviolet-complete Beyond Standard Model (BSM), the Minimal Supersymmetric Standard Model (MSSM) predicts two WIMP-like DM candidates in the form of sneutrino [8] or neutralino [9] when R-parity is imposed. For the left-handed sneutrino as the lightest supersymmetric particle (LSP), its interaction with the  $Z$  boson predicts a very small relic abundance relative to its measured value as well as an unacceptably large DM-nucleon scattering rate [10]. Consequently, the neutralino DM as the solely viable WIMP candidate has been intensively studied over the past decades. However, with the rapid progress in DM direct detection (DD) experiments (such as PandaX-II [11, 12], LUX [13] and XENON-1T [14, 15]) in recent years, it was found that the candidate became disfavored by the experiments [16–18] assuming that it is fully responsible for the measured DM relic density and that the Higgsino mass  $\mu$  is of  $\mathcal{O}(10^2 \text{ GeV})$ , which is favored by  $Z$  boson mass. This situation motivates us to consider DM physics in extended MSSM.

Besides the DM puzzle, the non-vanishing neutrino mass is another firm evidence on the existence of new physics [19]. Seesaw mechanism is the most popular way to generate the mass, and depending on the introduction of heavy neutrino fields, several variants of this mechanism, such as Type-I [20], -II [21], -III [22] and Inverse [23, 24] seesaw, have been proposed. Among these variants, the Type-I mechanism is the most economical one where only right-handed neutrino field is introduced. In the simplest supersymmetric realization of this mechanism, namely the MSSM with Type-I mechanism, a pure right-handed sneutrino LSP [25–28] or a mixed left- and right-handed sneutrino LSP [10, 29, 30] may act as a viable DM candidate. For the former case, the coupling of the candidate to ordinary matter is extremely suppressed either by neutrino Yukawa couplings or by the mass scale of the right-handed neutrino. As a result, its self- and co-annihilation cross sections are so tiny that it has to be non-thermal to avoid an overclosed universe [25–27]. For the latter case, a significant chiral mixture of the sneutrinos requires an unconventional supersymmetry breaking mechanism [29]. Furthermore, since the couplings of the DM candidate with the SM particles are determined by the mixing, it is difficult to predict simultaneously the right DM abundance and a suppressed DM-nucleon scattering rate required by the DM DD experiments [31–33]<sup>1</sup>. These facts reveal that the DM physics in Type-I MSSM is also unsatisfactory.

The situation may be changed greatly if one embeds the seesaw mechanism into the

---

<sup>1</sup>Numerically speaking, the mixing angle should satisfy  $\sin \theta_{\bar{\nu}} \sim 0.02$  for  $m_{\bar{\nu}} = 100 \text{ GeV}$  to predict the right DM relic density by the  $Z$  boson mediated annihilation, which corresponds to the scattering rate at the order of  $10^{-45} \text{ cm}^{-2}$  [33]. We find that the correlation between the relic density and the scattering rate is underestimated in Fig.1 of [34].

NMSSM, which, as one of most economical extensions of the MSSM, is characterized by predicting one gauge singlet Higgs superfield  $\hat{S}$ [35]. It has long been known that the field  $\hat{S}$  plays an extraordinary role in the model: solving the  $\mu$  problem of the MSSM[35], enhancing the theoretical prediction about the mass of the SM-like Higgs boson[36–38] as well as enriching the phenomenology of the NMSSM (see for example [39–44]). In this context we stress that, in the seesaw extension of the NMSSM, it is also responsible for heavy neutrino mass and the annihilation of sneutrino DM[45–47], and consequently makes the sneutrino DM compatible with various measurements. The underlying reason for the capability is that the newly introduced heavy neutrino fields in the extension are singlets under the gauge group of the SM model, so they can couple directly with  $\hat{S}$ . We also stress that the seesaw extension is essential not only to generate neutrino mass, but also to enrich greatly the phenomenology of the NMSSM given the very strong constraint of the recent DM DD experiments on neutralino DM in the NMSSM[48].

In our previous work[45], we augmented the NMSSM with inverse seesaw mechanism by introducing two types of gauge singlet chiral superfields  $\hat{\nu}_R$  and  $\hat{X}$ , which have lepton number  $-1$  and  $1$  respectively, and sketched the features of sneutrino DM. We found that, due to the assignment of the superfield’s charge under the SM gauge group, the scalar component fields of  $\hat{\nu}_R$ ,  $\hat{X}$  and  $\hat{S}$  compose a secluded DM sector, which can account for the measured DM relic abundance, and also be testable by future DM indirect detect experiments and LHC experiments. Since this sector communicates with the SM sector mainly through the small singlet-doublet Higgs mixing, the DM-nucleon scattering rate is naturally suppressed, which is consistent with current DM direct search results. We note that these features should be applied to the Type-I seesaw extension of the NMSSM due to the similarities of the two theoretical frameworks<sup>2</sup>. We also note that, in comparison with the inverse seesaw extension, the sneutrino sector in the Type-I seesaw extension involves less parameters, and thus is easier to be fully explored in practice. So as a preliminary work in our series of studies on sneutrino DM in different seesaw extensions of the NMSSM, we focus on the Type-I extension, and perform a rather sophisticated scan over the vast parameter space of the model by Nested Sampling method[49]. The relevant likelihood function is constructed from B-physics measurements, LHC Higgs data, DM relic density and its direct and indirect search limits, and statistic quantities are used to analyse the scan results. As far as we know, such an analysis of the Type-I seesaw extended NMSSM has not been done before, and new insights about the model are obtained. For example, we find that for most samples in the  $1\sigma$  regions of the posterior probability distribution function (PDF) on the plane of the sneutrino DM mass  $m_{\tilde{\nu}_1}$  versus the Higgsino mass  $\mu$ , the two masses are nearly degenerate. This is because the singlet Higgs field can mediate

---

<sup>2</sup>Generally speaking, the property of the sneutrino DM in the Type-I extension differs from that in the inverse seesaw extension only in two aspects. One is that in the Type-I extension, the sneutrino DM is a roughly pure right-handed sneutrino state, while in the inverse seesaw extension, it is a mixture of  $\tilde{\nu}_L$ ,  $\tilde{\nu}_R$  and  $\tilde{X}$  with the last two components being dominated. Consequently, the DM physics in the inverse seesaw extension is more complex[45–47]. The other is that in both the extensions, CP-even and CP-odd sneutrino states split in mass due to the presence of lepton number violating interactions. In the Type-I extension the splitting may be quite large, while in the other model, it tends to be smaller than about 1GeV.

the transition between the DM pair and the Higgsino pair, which implies that the DM and the Higgsinos can be in thermal equilibrium in early Universe before their freeze-out. If their mass splitting is less than about 10%, the number density of the Higgsinos can track that of the DM during freeze-out, and consequently the Higgsinos played an important role in determining DM relic density[50] (in literature such a phenomenon was called coannihilation [51]). As a result, even for very weak couplings of the DM with SM particles, the DM may still reach the correct relic density by coannihilating with the Higgsino-dominated particles. Such a possibility is not discussed in literatures. We also find that in many cases, the model does not need fine tuning to be consistent with the DM DD limits on the DM-nucleon scattering rate. This is a great advantage of the theory in light of the tightness of the limits, but it is not emphasized in literatures.

The Type-I extension of the NMSSM was firstly proposed in [52], and its DM physics was sketched in [53, 54]. Since then a lot of works appeared to study the phenomenology of the model[55–64]. For example, the spectral features of the  $\gamma$ -ray from DM annihilations were investigated in [55, 57, 58, 61, 62], and the Higgs physics was discussed in [56, 59]. We note that some of these studies focused on the parameter regions which predict a relatively large DM-nucleon scattering rate[53, 54]. These regions have now been excluded by the DM DD experiments, and thus the corresponding results are out of date. We also note that some other works were based on multi-component DM assumption, so they used the upper limit of the DM relic abundance as the criterion for parameter selection[55, 57, 58, 61]. Obviously, the conclusions obtained in this way are less definite than those with single DM candidate assumption. Given the incompleteness of the research in this field and also the great improvements of experimental limits on DM property in recent years, we are encouraged to carry out a comprehensive study on the key features of the model in this work.

This paper is organized as follows. In section 2, we first introduce briefly the basics of the NMSSM with Type-I seesaw extension, including its field content and Lagrangian, then we focus on the features of sneutrino sector. In Section 3, we perform a comprehensive scan over the vast parameter space of the model by considering various experimental measurements, and adopt statistic quantities to show the favored parameter space, DM annihilation mechanisms as well as the features of DM-nucleon scattering for the cases that the sneutrino DM is CP-even and CP-odd. Collider constraints on sneutrino DM scenarios are discussed in Section 4, and conclusions are presented in Section 5.

## 2 NMSSM with Type-I Mechanism

In this section we first recapitulate the basics of the NMSSM with Type-I mechanism, including its field content and Lagrangian, then we concentrate on sneutrino sector by analyzing sneutrino mass matrix, the annihilation mechanism of sneutrino DM and its scattering with nucleon.

SF	Spin 0	Spin $\frac{1}{2}$	Generations	$(U(1) \otimes SU(2) \otimes SU(3))$
$\hat{q}$	$\tilde{q}$	$q$	3	$(\frac{1}{6}, \mathbf{2}, \mathbf{3})$
$\hat{l}$	$\tilde{l}$	$l$	3	$(-\frac{1}{2}, \mathbf{2}, \mathbf{1})$
$\hat{H}_d$	$H_d$	$\tilde{H}_d$	1	$(-\frac{1}{2}, \mathbf{2}, \mathbf{1})$
$\hat{H}_u$	$H_u$	$\tilde{H}_u$	1	$(\frac{1}{2}, \mathbf{2}, \mathbf{1})$
$\hat{d}$	$\tilde{d}_R^*$	$d_R^*$	3	$(\frac{1}{3}, \mathbf{1}, \bar{\mathbf{3}})$
$\hat{u}$	$\tilde{u}_R^*$	$u_R^*$	3	$(-\frac{2}{3}, \mathbf{1}, \bar{\mathbf{3}})$
$\hat{e}$	$\tilde{e}_R^*$	$e_R^*$	3	$(1, \mathbf{1}, \mathbf{1})$
$\hat{s}$	$S$	$\tilde{S}$	1	$(0, \mathbf{1}, \mathbf{1})$
$\hat{\nu}$	$\tilde{\nu}_R^*$	$\nu_R^*$	3	$(0, \mathbf{1}, \mathbf{1})$

**Table 1.** Field content of the NMSSM with Type-I seesaw mechanism.

## 2.1 Model Lagrangian

As the simplest seesaw extension of the NMSSM, the NMSSM with Type-I seesaw mechanism introduces right-handed neutrino fields to generate neutrino mass. Consequently, the extension differs from the NMSSM only in neutrino/sneutrino sector, and the sneutrino DM as the lightest supersymmetric state in this sector couples mainly to Higgs bosons. With the field content presented in Table 1, the relevant superpotential and soft breaking terms are[53, 54]

$$\begin{aligned}
W &= W_F + \lambda \hat{s} \hat{H}_u \cdot \hat{H}_d + \frac{1}{3} \kappa \hat{s}^3 + \lambda_\nu \hat{s} \hat{\nu} \hat{\nu} + Y_\nu \hat{l} \cdot \hat{H}_u \hat{\nu}, \\
L_{soft} &= m_{H_d}^2 |H_d|^2 + m_{H_u}^2 |H_u|^2 + m_S^2 |S|^2 + m_\nu^2 \tilde{\nu}_R \tilde{\nu}_R^* \\
&\quad + (\lambda A_\lambda S H_u \cdot H_d + \frac{1}{3} \kappa A_\kappa S^3 + \lambda_\nu A_{\lambda_\nu} S \tilde{\nu}_R^* \tilde{\nu}_R^* + Y_\nu A_\nu \tilde{\nu}_R^* \tilde{l} H_u + \text{h.c.}) + \dots \quad (2.1)
\end{aligned}$$

where  $W_F$  denotes the superpotential of the MSSM without  $\mu$  term, and we have imposed a  $Z_3$  symmetry to forbid the appearance of any dimensional parameters in  $W$ . In above formulae, the coefficients  $\lambda$  and  $\kappa$  parameterize the interactions among the Higgs fields,  $Y_\nu$  and  $\lambda_\nu$  are neutrino Yukawa couplings with flavor index omitted,  $m_i$  ( $i = H_u, H_d, \dots$ ) denote soft breaking masses, and  $A_i$  ( $i = \lambda, \kappa, \dots$ ) are soft breaking coefficients for trilinear terms. Since the soft breaking squared masses  $m_{H_u}^2$ ,  $m_{H_d}^2$  and  $m_S^2$  are related with the vacuum expectation values of the fields  $H_u$ ,  $H_d$  and  $S$ ,  $\langle H_u \rangle = v_u/\sqrt{2}$ ,  $\langle H_d \rangle = v_d/\sqrt{2}$  and  $\langle S \rangle = v_s/\sqrt{2}$ , by the minimization conditions of the Higgs potential after the electroweak symmetry breaking[35], in practice one usually takes  $\lambda$ ,  $\kappa$ ,  $\tan \beta \equiv v_u/v_d$ ,  $A_\lambda$ ,  $A_\kappa$  and  $\mu \equiv \lambda v_s/\sqrt{2}$  as theoretical input parameters for Higgs sector.

The model predicts three CP-even Higgs mass eigenstates  $h_i$  with  $i = 1, 2, 3$  and two CP-odd mass eigenstates  $A_1$  and  $A_2$ , which are the mixtures of the real and imaginary parts of the fields  $H_u^0$ ,  $H_d^0$  and  $S$ , respectively. Throughout this paper, we assume the mass order  $m_{h_1} < m_{h_2} < m_{h_3}$  and  $m_{A_1} < m_{A_2}$ . It also predicts a pair of charged Higgs  $H^\pm$  which are given by  $H^\pm = \cos \beta H_u^\pm + \sin \beta H_d^\pm$ . Among these physical states, one of the CP-even state corresponds to the SM-like Higgs boson discovered at the LHC, and its measured property has tightly limited the input parameters in the Higgs sector. In particular, it requires that

the state should be  $Re(H_u^0)$  dominated if  $m_{H^\pm} \gg v$  and  $\tan \beta \gg 1$ . The heavier doublet-dominated CP-even state is roughly degenerate in mass with the doublet-dominated CP-odd state and also with the charged states, and the LHC search for extra Higgs bosons together with the indirect constraints from  $B$ -physics have required  $m_{H^\pm} \gtrsim 0.8\text{TeV}$ , which is quite similar to MSSM case[65]. Moreover, the doublet-dominated states couple with the sneutrino DM via the interaction  $\lambda\lambda_\nu H_u \cdot H_d \tilde{\nu}_R^* \tilde{\nu}_R^* + h.c.$ , which is induced by the F-term of the Lagrangian. In the limit  $m_{H^\pm} \rightarrow \infty$ , only the SM-like Higgs boson plays a role in DM physics, but since its interaction with sneutrino pair is proportional to  $\lambda\lambda_\nu v_d$ , its effect is usually not important. As for the singlet-dominated CP-even and CP-odd states, collider constraints on them are rather weak and consequently they may be light. These states couple with sneutrino pair with three or four scalar interaction induced by the  $\lambda_\nu \hat{s} \hat{\nu} \hat{\nu}$  term in the superpotential and its soft breaking term. Consequently, the states can act as the annihilation product of the sneutrino DM or mediate the annihilation. So they play an important role in DM annihilation.

## 2.2 Sneutrino mass

In the NMSSM with Type-I seesaw extension, the active neutrino mass matrix is given by  $m_\nu = y_\nu v_u M^{-1} y_\nu^T v_u$  with  $M = 2\lambda_\nu v_S$  denoting the heavy neutrino mass matrix[52]. Since the mass scale of the active neutrinos is  $\sim 0.1\text{eV}$ , the magnitude of  $Y_\nu$  should be about  $10^{-6}$  for the scale of  $M$  around  $100\text{GeV}$ . In order to reproduce neutrino oscillation data,  $m_\nu$  must be flavor non-diagonal, which can be realized by assuming that the Yukawa coupling  $Y_\nu$  is non-diagonal, while  $\lambda_\nu$  is diagonal. If one further assumes that the soft breaking parameters in sneutrino sector, such as  $m_{\tilde{\nu}}$ ,  $m_\nu$  and  $A_{\lambda_\nu}$ , are flavor diagonal, the flavor mixings of sneutrinos are then extremely suppressed by the off-diagonal elements of  $Y_\nu$ . In this case, it is enough to only consider one generation case in studying the properties of the sneutrino DM, which is what we will do in following discussion.

After decomposing sneutrino fields into CP-even and CP-odd parts:

$$\tilde{\nu}_L \equiv \frac{1}{\sqrt{2}}(\tilde{\nu}_{L1} + i\tilde{\nu}_{L2}), \quad \tilde{\nu}_R \equiv \frac{1}{\sqrt{2}}(\tilde{\nu}_{R1} + i\tilde{\nu}_{R2}), \quad (2.2)$$

one can write down the sneutrino mass matrix in the basis  $(\tilde{\nu}_{L1}, \tilde{\nu}_{R1}, \tilde{\nu}_{L2}, \tilde{\nu}_{R2})$  as follows

$$\mathcal{M}_\nu^2 = \begin{pmatrix} m_{L\bar{L}}^2 & \frac{m_{LR}^2 + m_{L\bar{R}}^2 + c.c.}{2} & 0 & i\frac{m_{LR}^2 - m_{L\bar{R}}^2 - c.c.}{2} \\ \frac{m_{LR}^2 + m_{L\bar{R}}^2 + c.c.}{2} & m_{R\bar{R}}^2 + m_{RR}^2 + m_{RR}^{2*} & i\frac{m_{LR}^2 - m_{L\bar{R}}^2 - c.c.}{2} & i(m_{RR}^2 - m_{RR}^{2*}) \\ 0 & i\frac{m_{LR}^2 - m_{L\bar{R}}^2 - c.c.}{2} & m_{L\bar{L}}^2 & \frac{-m_{LR}^2 + m_{L\bar{R}}^2 + c.c.}{2} \\ i\frac{m_{LR}^2 - m_{L\bar{R}}^2 - c.c.}{2} & i(m_{RR}^2 - m_{RR}^{2*}) & \frac{-m_{LR}^2 + m_{L\bar{R}}^2 + c.c.}{2} & m_{R\bar{R}}^2 - m_{RR}^2 - m_{RR}^{2*} \end{pmatrix},$$

where

$$\begin{aligned} m_{L\bar{L}}^2 &\equiv m_{\tilde{\nu}}^2 + |y_\nu v_u|^2 + \frac{1}{8}(g_1^2 + g_2^2)(v_d^2 - v_u^2), \\ m_{LR}^2 &\equiv y_\nu (-\lambda v_s v_d)^* + y_\nu A_{y_\nu} v_u, \\ m_{L\bar{R}}^2 &\equiv y_\nu v_u (-\lambda v_s)^*, \\ m_{R\bar{R}}^2 &\equiv m_\nu^2 + |2\lambda_\nu v_s|^2 + |y_\nu v_u|^2, \\ m_{RR}^2 &\equiv \lambda_\nu (A_{\lambda_\nu} v_s + (\kappa v_s^2 - \lambda v_d v_u)^*). \end{aligned} \quad (2.3)$$

If all the parameters in the matrix are real, namely there is no CP violation, the real and imaginary parts of the sneutrino fields will not mix and the mass term can be split as follows

$$\begin{aligned} & \frac{1}{2}(\tilde{\nu}_{L1}, \tilde{\nu}_{R1}) \begin{pmatrix} m_{L\bar{L}}^2 & m_{LR}^2 + m_{L\bar{R}}^2 \\ m_{LR}^2 + m_{L\bar{R}}^2 & m_{R\bar{R}}^2 + 2m_{RR}^2 \end{pmatrix} \begin{pmatrix} \tilde{\nu}_{L1} \\ \tilde{\nu}_{R1} \end{pmatrix} \\ & + \frac{1}{2}(\tilde{\nu}_{L2}, \tilde{\nu}_{R2}) \begin{pmatrix} m_{L\bar{L}}^2 & -m_{LR}^2 + m_{L\bar{R}}^2 \\ -m_{LR}^2 + m_{L\bar{R}}^2 & m_{R\bar{R}}^2 - 2m_{RR}^2 \end{pmatrix} \begin{pmatrix} \tilde{\nu}_{L2} \\ \tilde{\nu}_{R2} \end{pmatrix}. \end{aligned} \quad (2.4)$$

From this formula, one can learn that the chiral mixings of the sneutrinos are proportional to  $y_\nu$ , and hence can be ignored safely. So sneutrino mass eigenstate coincides with chiral state. In our study, the sneutrino DM corresponds to the lightest right-handed sneutrino. One can also learn that the mass splitting between the CP-even and CP-odd right-handed states is given by  $\Delta m^2 \equiv m_{even}^2 - m_{odd}^2 = 4m_{RR}^2$ , which implies that the CP-even state  $\tilde{\nu}_{R1}$  is lighter than the CP-odd state  $\tilde{\nu}_{R2}$  if  $m_{RR}^2 < 0$  and vice versa. This implies that the sneutrino DM may be either CP-even or CP-odd. In this work, we consider both the possibilities.

Once the form of the sneutrino DM  $\tilde{\nu}_1$  is given, one can determine its coupling strength with  $h_i$ , which is given by

$$\begin{aligned} C_{\tilde{\nu}_1 \tilde{\nu}_1 h_i} &= \frac{2\lambda\lambda_\nu M_W}{\sqrt{2}g} (\sin\beta Z_{i1} + \cos\beta Z_{i2}) + \\ & \left[ \frac{\sqrt{2}}{\lambda} (4\lambda_\nu^2 + 2\kappa\lambda_\nu) \mu + \frac{\lambda_\nu A_{\lambda_\nu}}{\sqrt{2}} \right] Z_{i3}, \end{aligned} \quad (2.5)$$

where  $Z_{ij}$  ( $i, j = 1, 2, 3$ ) are the elements of the matrix to diagonalize the CP-even Higgs mass matrix in the basis  $(Re(H_d^0), Re(H_u^0), Re(S))$ . As is expected, this coupling is suppressed by  $\cos\beta$  if  $h_i$  is  $Re(H_u^0)$  dominant, but unsuppressed if it is  $Re(S)$  dominant.

### 2.3 DM Relic density

It is well known that the WIMP's relic abundance is related to its thermal averaged annihilation cross section at the time of freeze-out [9]. In order to obtain the WIMP's abundance one should solve following Boltzmann equation,

$$\frac{dY}{dT} = \sqrt{\frac{\pi g_*(T)}{45}} M_p - \langle\sigma v\rangle (Y^2 - Y_{eq}^2), \quad (2.6)$$

where  $g_*$  is the effective number of degrees of freedom at thermal equilibrium,  $M_p$  is the Plank mass,  $Y$  and  $Y_{eq}$  are the relic abundance and the thermal equilibrium abundance respectively, and  $\langle\sigma v\rangle$  is WIMP's relativistic thermal averaged annihilation cross section with  $v$  denoting the relative velocity between the annihilating particles.  $\langle\sigma v\rangle$  is related to the particle physics model by[66],

$$\langle\sigma v\rangle = \frac{\sum_{i,j} g_i g_j \int_{(m_i+m_j)^2} ds \sqrt{s} K_1\left(\frac{\sqrt{s}}{T}\right) p_{ij}^2 \sum_{k,l} \sigma_{ij;kl}(s)}{2T \left(\sum_i g_i m_i^2 K_2(m_i/T)\right)^2}, \quad (2.7)$$

where  $g_i$  is the number of degrees of freedom,  $\sigma_{ij;kl}$  is the cross section for annihilation of a pair of particles with masses  $m_i$  and  $m_j$  into SM particles  $k$  and  $l$ ,  $p_{ij}$  is the momentum of incoming particles in their center of mass frame with squared total energy  $s$ , and  $K_i$  ( $i = 1, 2$ ) are modified Bessel functions.

The present day abundance is obtained by integrating Eq.(2.6) from  $T = \infty$  to  $T = T_0$ , where  $T_0$  is the temperature of the Universe today. And WIMP relic density can be written as [66],

$$\Omega h^2 = 2.742 \times 10^8 \frac{M_{WIMP}}{\text{GeV}} Y(T_0). \quad (2.8)$$

In the NMSSM with Type-I seesaw mechanism, possible annihilation channels of the sneutrino DM include[53, 54]

- (1)  $\tilde{\nu}_1 \tilde{\nu}_1 \rightarrow VV^*, VS, f\bar{f}$  with  $V, S$  and  $f$  denoting a vector boson ( $W$  or  $Z$ ), a Higgs boson and a SM fermion, respectively. This kind of annihilations proceed via  $s$ -channel exchange of a CP-even Higgs boson.
- (2)  $\tilde{\nu}_1 \tilde{\nu}_1 \rightarrow SS^*$  via  $s$ -channel Higgs exchange,  $t/u$ -channel sneutrino exchange, and relevant scalar quartic couplings.
- (3)  $\tilde{\nu}_1 \tilde{\nu}_1 \rightarrow \nu_R \bar{\nu}_R$  via  $s$ -channel Higgs exchange and  $t/u$ -channel neutralino exchange.
- (4)  $\tilde{\nu}_1 \tilde{\nu}'_1 \rightarrow A_i^{(*)} \rightarrow XY$  with  $\tilde{\nu}'_1$  denoting a right-handed sneutrino with an opposite CP number to that of  $\tilde{\nu}_1$ , and  $X$  and  $Y$  denoting any possible light state. This annihilation channel is important in determining the relic density only when the CP-even and CP-odd states are nearly degenerate in mass.
- (5)  $\tilde{\nu}_1 \tilde{\nu}_1 \rightarrow \tilde{\chi}^0 \tilde{\chi}^0, \tilde{\chi}^\pm \tilde{\chi}^\pm \rightarrow XY$ . This annihilation is called coannihilation[50, 51], and it becomes important if the mass splitting between  $\tilde{\chi}$  and  $\tilde{\nu}_1$  is less than about 10%.

The expressions of  $\sigma v$  for some of the channels are presented in [54]. One can learn from them that  $\lambda_\nu, A_\nu, m_\nu^2$  as well as the parameters in Higgs sector are involved in the annihilations<sup>3</sup>.

## 2.4 DM Direct detection

Since  $\tilde{\nu}_1$  in this work is a right-handed scalar with definite CP and lepton numbers, its scattering with nucleon  $N$  ( $N = p, n$ ) proceeds only by exchanging CP-even Higgs bosons. In the non-relativistic limit, this process is described by an effective operator  $\mathcal{L}_{\tilde{\nu}_1 N} = f_N \tilde{\nu}_1 \tilde{\nu}_1 \bar{\psi}_N \psi_N$  with the coefficient  $f_N$  given by [67]

$$f_N = m_N \sum_{i=1}^3 \frac{C_{\tilde{\nu}_1 \tilde{\nu}_1 h_i} C_{NN h_i}}{m_{h_i}^2} = m_N \sum_{i=1}^3 \frac{C_{\tilde{\nu}_1 \tilde{\nu}_1 h_i}}{m_{h_i}^2} \frac{(-g)}{2m_W} \left( \frac{Z_{i2}}{\sin \beta} F_u^{(N)} + \frac{Z_{i1}}{\cos \beta} F_d^{(N)} \right),$$

where  $C_{NN h_i}$  denotes the Yukawa coupling of the Higgs boson  $h_i$  with nucleon  $N$ , and  $F_u^{(N)} = f_u^{(N)} + \frac{4}{27} f_G^{(N)}$  and  $F_d^{(N)} = f_d^{(N)} + f_s^{(N)} + \frac{2}{27} f_G^{(N)}$  are nucleon form factors with

<sup>3</sup>We note that the works [53, 54] failed to consider the annihilation channels (4) and (5). Especially, the channel (5) is testified to be most important by our following study. We also note that in calculating  $\sigma v$  of the channel  $\tilde{\nu}_1 \tilde{\nu}_1 \rightarrow A_i A_j$ , the authors neglected the contribution from the  $t/u$ -channel sneutrino exchange.

$f_q^{(N)} = m_N^{-1} \langle N | m_q q \bar{q} | N \rangle$  (for  $q = u, d, s$ ) and  $f_G^{(N)} = 1 - \sum_{q=u,d,s} f_q^{(N)}$ . Consequently, the spin-dependent cross section for the scattering vanishes, and the spin independent cross section is given by[67]

$$\sigma_{\tilde{\nu}_1-N}^{\text{SI}} = \frac{\mu_{\text{red}}^2}{4\pi m_{\tilde{\nu}_1}^2} f_N^2 = \frac{4F_u^{(N)2} \mu_{\text{red}}^2 m_N^2}{\pi} \left( \sum_i \xi_i \right)^2, \quad (2.9)$$

where  $\mu_{\text{red}} = m_N / (1 + m_N^2 / m_{\tilde{\nu}_1}^2)$  is the reduced mass of the nucleon with  $m_{\tilde{\nu}_1}$ , and  $\xi_i$  with  $i = 1, 2, 3$  are defined by

$$\xi_i = -\frac{g}{8m_W} \frac{C_{\tilde{\nu}_1 \tilde{\nu}_1 h_i}}{m_{h_i}^2 m_{\tilde{\nu}_1}} \left( \frac{Z_{i2}}{\sin \beta} + \frac{Z_{i1}}{\cos \beta} \frac{F_d^{(N)}}{F_u^{(N)}} \right) \quad (2.10)$$

to facilitate our analysis. Obviously,  $\xi_i$  represents the  $h_i$  contribution to the cross section.

In our numerical calculation of the DM-proton scattering rate  $\sigma_{\tilde{\nu}_1-p}^{\text{SI}}$ , we use the default setting of the package micrOMEGAs [66, 70, 71] for the nucleon form factors,  $\sigma_{\pi N} = 34\text{MeV}$  and  $\sigma_0 = 42\text{MeV}$ , and obtain  $F_u^{(p)} \simeq 0.15$  and  $F_d^{(p)} \simeq 0.14$ <sup>4</sup>. In this case, Eq.(2.9) can be approximated by

$$\sigma_{\tilde{\nu}_1-p}^{\text{SI}} \simeq \frac{4F_u^{(p)2} \mu_{\text{red}}^2 m_p^2}{\pi} \left\{ \frac{g}{8m_W} \sum_i \left[ \frac{C_{\tilde{\nu}_1 \tilde{\nu}_1 h_i}}{m_{h_i}^2 m_{\tilde{\nu}_1}} \left( \frac{Z_{i2}}{\sin \beta} + \frac{Z_{i1}}{\cos \beta} \right) \right] \right\}^2. \quad (2.11)$$

From this approximation and also the expression of  $C_{\tilde{\nu}_1 \tilde{\nu}_1 h_i}$  in Eq.(2.5), one can get following important features about the scattering of the sneutrino DM with nucleon:

- For each of the  $h_i$  contributions, it depends not only on the parameters in Higgs sector, but also on the parameters in sneutrino sector such as  $\lambda_\nu$  and  $A_{\lambda_\nu}$ . This feature lets the theory have a great degree of freedom to adjust the contribution size so that the severe cancellation among the contributions can be easily achieved. By contrast, in the NMSSM with neutralino as a DM candidate, the contribution depends on, beside the DM mass, only the parameters in Higgs sector, and consequently it is not easy to reach the blind spot for DM-nucleon scattering due to the tight constraints on the Higgs parameters from LHC experiments[72–75].
- Each of the  $h_i$  contributions can be suppressed. To be more specific, the  $Re(H_d^0)$  dominated Higgs is usually at TeV scale, so its contribution is suppressed by the squared mass; the  $Re(H_u^0)$  dominated scalar corresponds to the SM-like Higgs boson, and its coupling with  $\tilde{\nu}_1$  can be suppressed by  $\cos \beta$  and/or by the accidental cancellation among different terms in  $C_{\tilde{\nu}_1 \tilde{\nu}_1 h_i}$ . In most cases, the contribution from the singlet-dominated scalar is most important, but such a contribution is obviously suppressed by the doublet-singlet mixing in the scalar.

<sup>4</sup>Note that different choices of the pion-nucleon sigma term  $\sigma_{\pi N}$  and  $\sigma_0$  can induce an uncertainty of  $\mathcal{O}(10\%)$  on  $F_u^{(p)}$  and  $F_d^{(p)}$ . For example, if one takes  $\sigma_{\pi N} = 59\text{MeV}$  and  $\sigma_0 = 57\text{MeV}$ , which are determined from [68] and [69] respectively,  $F_u^{(p)} \simeq 0.16$  and  $F_d^{(p)} \simeq 0.13$ .

Parameter	Value	Parameter	Value	Parameter	Value
$m_{\tilde{q}}$	$2\text{TeV} \times \mathbf{1}$	$A_{u,c,d,s}$	2TeV	$A_\lambda$	2TeV
$m_{\tilde{l}}$	$0.4\text{TeV} \times \mathbf{1}$	$A_{e,\mu,\tau}$	0.4TeV	$y_\nu$	$10^{-6} \times \mathbf{1}$
$M_1$	0.4TeV	$M_2$	0.8TeV	$M_3$	2.4TeV

**Table 2.** Fixed parameters in the seesaw extension of the NMSSM.  $m_{\tilde{q}}$  for  $\tilde{q} = \tilde{Q}, \tilde{U}, \tilde{D}$  and  $m_{\tilde{l}}$  for  $\tilde{l} = \tilde{L}, \tilde{E}$  denote soft masses of squarks and sleptons, respectively, with  $\mathbf{1}$  being unit matrix in flavor space, and  $M_i$  with  $i = 1, 2, 3$  are soft masses for gauginos.  $A_i$  with  $i = u, c, d, s, e, \mu, \tau$  are coefficients of soft trilinear terms for a specific flavor, and the other flavor changing trilinear coefficients are assumed to be zero.

We emphasize that these features make the theory compatible with the strong constraints from the DM DD experiments in broad parameter spaces. In order to parameterize the degree of the cancellation among the contributions, we define the fine tuning quantity  $\Delta_{FT}$  as

$$\Delta_{FT} = \max_i \left\{ \frac{\xi_i^2}{(\sum_i \xi_i)^2} \right\}. \quad (2.12)$$

Obviously,  $\Delta_{FT} \sim 1$  is the most ideal case for any DM theory in predicting an experimentally allowed  $\sigma_{\tilde{\nu}_1-p}^{\text{SI}}$ , and the larger  $\Delta_{FT}$  becomes, the more unnatural the theory is.

### 3 Numerical Results

In our study of the sneutrino DM scenarios, we utilize the package SARAH-4.11.0 [76–78] to build the model, the codes SPheno-4.0.3[79] and FlavorKit[80] to generate the particle spectrum and compute low energy flavor observables, respectively, and the package MicrOMEGAs 4.3.4[66, 70, 71] to calculate DM observables by assuming that the lightest sneutrino is the sole DM candidate in the universe. We also consider the bounds from the direct searches for Higgs bosons at LEP, Tevatron and LHC by the packages HiggsBounds-5.0.0[81] and HiggsSignal-2.0.0 [82].

#### 3.1 Scan strategy

Previous discussion indicates that only the parameters in Higgs sector and sneutrino sector are involved in the DM physics. We perform a sophisticated scan over these parameters in following ranges:

$$\begin{aligned} 0 < \lambda_\nu \leq 0.5, \quad 0 < \lambda \leq 0.7, \quad |\kappa| \leq 0.7, \quad 1 \leq \tan\beta \leq 60, \quad |A_{\lambda_\nu}|, |A_\kappa| \leq 1\text{TeV}, \\ 100\text{GeV} \leq \mu \leq 300\text{GeV}, \quad 0 \leq m_{\tilde{\nu}} \leq 300\text{GeV}, \quad |A_t| \leq 5\text{TeV}, \end{aligned} \quad (3.1)$$

by setting  $A_b = A_t$  and other unimportant parameters in Table 2. All the parameters are defined at the scale  $Q = 1\text{TeV}$ . Our interest in the parameter space is due to following considerations:

- Since the masses of the heavy doublet-dominated Higgs bosons are usually at TeV scale, which is favored by direct searches for extra Higgs boson at the LHC, their

effects on the DM physics are decoupled and thus become unimportant. We here fix the parameter  $A_\lambda$ , which is closely related with  $m_{H^\pm}$ [35], at 2TeV to simplify the calculation given that the scan is very time-consuming for computer clusters. Consequently, we find that the Higgs bosons are heavier than about 1TeV for almost all samples.

- It is well known that the radiative correction from top/stop and bottom/sbottom loops to the Higgs mass spectrum plays an important role for SUSY to coincide with experimental measurements. In our calculation, we include such an effect by fixing  $m_{\tilde{Q}_3} = m_{\tilde{U}_3} = m_{\tilde{D}_3} = 2\text{TeV}$  and varying  $A_{t,b}$  over a broad region,  $|A_t| \leq 5\text{TeV}$ . We remind that within the region, the color and charge symmetries of the theory remain unbroken[83, 84].
- The upper bounds of the parameters  $\lambda$ ,  $\kappa$ ,  $\lambda_\nu$  and  $\tan\beta$  coincide with the perturbativity of the theory up to Planck scale[35].
- Because the Higgsino mass  $\mu$  is directly related to  $Z$  boson mass, naturalness prefers  $\mu \sim \mathcal{O}(10^2\text{GeV})$ [35]. So we require  $100\text{GeV} \leq \mu \leq 300\text{GeV}$ , where the lower bound comes from the LEP search for chargino and neutralinos, and the upper bound is imposed by hand.
- Since the sneutrino DM must be lighter than the Higgsino, its soft breaking mass  $m_{\tilde{\nu}}$  is therefore upper bounded by about 300GeV.
- In order to get correct EWSB and meanwhile predict the masses of the singlet dominated scalars around 100GeV,  $|A_{\lambda_\nu}|$  and  $|A_\kappa|$  can not be excessively large from naturalness argument.
- We require the other dimensional parameters sufficiently large so that their prediction on sparticle spectrum is consistent with the results of the direct search for sparticles at the LHC.

In order to make the conclusions obtained in this work as complete as possible, we adopt the MultiNest algorithm[49], which is implemented in our code EasyScan\_HEP[85], with more than  $5 \times 10^7$  physical samples computed in the scan. The output of the scan includes the Bayesian evidence defined by

$$Z(D|M) \equiv \int P(D|O(M, \Theta))P(\Theta|M) \prod d\theta_i,$$

where  $P(\Theta|M)$  is called prior probability density function (PDF) for the parameters  $\Theta = (\Theta_1, \Theta_2, \dots)$  in the model  $M$ , and  $P(D|O(M, \Theta)) \equiv \mathcal{L}(\Theta)$  is the likelihood function for the theoretical predictions on the observables  $O$  confronted with their experimental measurements  $D$ . Computationally, the evidence is an average likelihood, and it depends on the priors for the model's parameters. For different scenarios in one theory, the larger  $Z$  is, the more readily the corresponding scenario agrees with the data. The output also

includes weighted and unweighted parameter samples which are subject to the posterior PDF  $P(\Theta|M, D)$ . This PDF is given by

$$P(\Theta|M, D) = \frac{P(D|O(M, \Theta))P(\Theta|M)}{Z}, \quad (3.2)$$

and it reflects the state of our knowledge about the parameters  $\Theta$  given the experimental data  $D$ , or alternatively speaking, the updated prior PDF after considering the impact of the experimental data. This quantity may be sensitive to the shape of the prior, but the sensitivity can be counterbalanced by sufficient data and thus lost[86]. Obviously, one can infer from the distribution of the samples the underlying physics of the model.

In the scan, we take flat distribution for the parameters  $\lambda$  and  $\kappa$ , and log distribution for the rest input parameters, which is widely adopted in literatures to set the prior PDF in scanning the parameter space of a BSM theory (see for example [87])<sup>5</sup>. The likelihood function we construct contains

$$\mathcal{L}(\Theta) = \mathcal{L}_{Higgs} \times \mathcal{L}_{Br(B_s \rightarrow \mu^+ \mu^-)} \times \mathcal{L}_{Br(B_s \rightarrow X_s \gamma)} \times \mathcal{L}_{\Omega_{\tilde{\nu}_1}} \times \mathcal{L}_{DD} \times \mathcal{L}_{ID}, \quad (3.3)$$

where each contribution on the right side of the equation is given as follows<sup>6</sup>:

- For the likelihood function of the Higgs searches at colliders,

$$\mathcal{L}_{Higgs} = e^{-\frac{1}{2}(\chi^2 + A^2)}, \quad (3.4)$$

where  $\chi^2$  comes from the fit of the theoretical prediction on the properties of the SM-like Higgs boson to relevant LHC data with its value calculated by the code HiggsSignal [82], and  $A^2$  reflects whether the parameter point is allowed or excluded by the direct searches for extra Higgs at colliders. In practice, we set by the output of the code HiggsBounds[81] either  $A^2 = 0$  (experimentally allowed) or  $A^2 = 400$  (an arbitrary large number, corresponding to the case of being experimentally excluded).

Since the Bayesian evidence for the scenario where  $h_1$  acts as the SM-like Higgs boson is much larger than that of the scenario with  $h_2$  corresponding to the SM-like Higgs boson[37, 38], **we in this work only consider the case that  $h_1$  corresponds to the Higgs boson discovered at the LHC, and present our results by the CP property of the sneutrino DM.**

- For the second, third and fourth contributions, i.e. the likelihood functions about the measurements of  $Br(B_s \rightarrow \mu^+ \mu^-)$ ,  $Br(B_s \rightarrow X_s \gamma)$  and DM relic density  $\Omega_{\tilde{\nu}_1}$ , they are Gaussian distributed. Specifically, any of them has the form

$$\mathcal{L} = e^{-\frac{[\mathcal{O}_{th} - \mathcal{O}_{exp}]^2}{2\sigma^2}}, \quad (3.5)$$

where  $\mathcal{O}_{th}$  denotes the theoretical prediction of the observable  $\mathcal{O}$ ,  $\mathcal{O}_{exp}$  represents its experimental central value and  $\sigma$  is the total (including both theoretical and experimental) uncertainties.

---

<sup>5</sup>Dimensional parameters usually span wide ranges, and if one sets them flat distribution, the efficiency of the scan will be lowered significantly.

<sup>6</sup>In practice, one usually encounters the nonphysical situation where the squared mass of any scalar particle is negative. In this case, we set the likelihood function to be sufficiently small, e.g.  $e^{-100}$ .

- For the likelihood function of DM DD experiments  $\mathcal{L}_{DD}$ , we take a Gaussian form with a mean value of zero[88]:

$$\mathcal{L} = e^{-\frac{\sigma^2}{2\delta_\sigma^2}}, \quad (3.6)$$

where  $\sigma$  stands for DM-nucleon scattering rate, and  $\delta_\sigma$  is evaluated by the formula  $\delta_\sigma^2 = UL_\sigma^2/1.64^2 + (0.2\sigma)^2$  with  $UL_\sigma$  denoting the upper limit of the latest XENON1T results on  $\sigma$  at 90% confidence level[15], and  $0.2\sigma$  parameterizing theoretical uncertainties.

- For the likelihood function of DM indirect search results from dwarf galaxies  $\mathcal{L}_{ID}$ , we use the data provided by Fermi-LAT collaboration [89], and adopt the likelihood function proposed in [90, 91]. Note that we do not consider the constraint on line signal of  $\gamma$ -ray from Fermi-LAT data since it is rather weak[92].

Given the posterior PDF and the likelihood function, one can obtain statistic quantities such as marginal posterior PDF and profile likelihood function (PL). The marginal posterior PDF for a given set of parameters  $(\Theta_A, \Theta_B, \dots)$  is defined by integrating the posterior PDF  $P(\Theta|M, D)$  in Eq.(3.2) over the rest model parameters. For example, the one-dimensional (1D) and two-dimensional (2D) marginal posterior PDFs are given by

$$P(\Theta_A|D) = \int P(\Theta|M, D)d\Theta_1d\Theta_2 \cdots d\Theta_{A-1}d\Theta_{A+1} \cdots, \quad (3.7)$$

$$P(\Theta_A, \Theta_B|D) = \int P(\Theta|M, D)d\Theta_1d\Theta_2 \cdots d\Theta_{A-1}d\Theta_{A+1} \cdots d\Theta_{B-1}d\Theta_{B+1} \cdots. \quad (3.8)$$

In practice, these PDFs are calculated by the sum of weighted samples in a chain with user-defined bins, and their densities as a function of  $\Theta_A$  and  $(\Theta_A, \Theta_B)$  respectively reflect the preference of the samples obtained in the scan. On the other hand, the frequentist PL is defined as the largest likelihood value in a certain parameter space. Taken the 1D and 2D PLs as an example, we get them by the procedure

$$\mathcal{L}(\Theta_A) = \max_{\Theta_1, \dots, \Theta_{A-1}, \Theta_{A+1}, \dots} \mathcal{L}(\Theta), \quad (3.9)$$

$$\mathcal{L}(\Theta_A, \Theta_B) = \max_{\Theta_1, \dots, \Theta_{A-1}, \Theta_{A+1}, \dots, \Theta_{B-1}, \Theta_{B+1}, \dots} \mathcal{L}(\Theta). \quad (3.10)$$

Obviously, PL reflects the preference of the theory on the parameter space, and for a given point in  $\Theta_A - \Theta_B$  plane, the value of  $\mathcal{L}(\Theta_A, \Theta_B)$  represents the capability of the point in the theory to account for experimental data. In following section, we display our results by these quantities. We also use other statistic quantities, such as  $1\sigma$  and  $2\sigma$  credible regions (CRs),  $1\sigma$  and  $2\sigma$  confidence intervals (CIs), and posterior mean, median and mode, to illustrate the features of the sneutrino DM scenario. The definition of these quantities can be found in the appendix of [93], and we use the package Superplot[93] with kernel density estimation to get them.

### 3.2 Favored parameter regions

In this subsection, we discuss favored parameter space for the case that the sneutrino DM is CP-even. In the left-panels of Fig.1 and Fig.2, we show the dependencies of the 1D

marginal PDF and PL on  $\lambda$ ,  $\kappa$ ,  $\tan\beta$ ,  $A_\kappa$ ,  $A_t$ ,  $\lambda_\nu$ ,  $A_{\lambda_\nu}$  and  $m_\nu$  respectively. We also present 2D results in Fig.3 on  $\kappa - \lambda$ ,  $\tan\beta - \lambda$ ,  $A_\kappa - \lambda$  and  $\mu - \lambda$  planes with color bars representing marginal posterior PDFs for the left panels and PLs for the right panels. The  $1\sigma$  and  $2\sigma$  CRs, the  $1\sigma$  and  $2\sigma$  CIs together with best fit point, posterior mean, median and mode are also shown in these panels. From the  $1\sigma$  CRs in these figures, one can learn following features:

- A relatively large  $\tan\beta$ , i.e.  $10 \lesssim \tan\beta \lesssim 35$ , is preferred. One reason for this is that, since  $\lambda$  in the scenario is usually less than about 0.35, a large  $\tan\beta$  is helpful to enhance the tree level prediction of the SM-like Higgs boson mass[35].
- A moderately small range of  $|A_\kappa| \leq 100\text{GeV}$  is favored. In this case,  $A_1$  tends to be light[35], and consequently it may sever as the product of the annihilation of the sneutrino DM, which will be discussed in next subsection.
- Although we vary the Higgsino mass  $\mu$  in a wide range from 100GeV to 300GeV, the mass tends to be less than about 220GeV, which is favored by predicting  $Z$  boson mass in a natural way[35]. We take this feature as an unanticipated advantage of the theory. One possible reason is that the DM usually coannihilated with the Higgsinos in early universe to get its right relic density (see discussion below), which requires the Higgsinos to be nearly degenerate in mass with the DM, and consequently heavy Higgsinos are not favored.
- For each input parameter, the range covered by the  $1\sigma$  CR is significantly less than that of the  $1\sigma$  CI. This difference is caused by the fact that the CR defined in Eq.(3.7) is determined not only by the likelihood function, but also by the parameter space. By contrast, the CI is affected only by the likelihood function.

Moreover, we emphasize that both the CR and the CI are determined by the total likelihood function, not by any individual contribution. For a good theory, the optimal parameter space for one component of the likelihood function should be compatible with that for the other components of the function so that the Bayesian evidence of the theory is not suppressed. So far as the Type-I seesaw extension is concerned, we once compared the  $1\sigma$  CRs in Fig.1 with those obtained from another independent scan of the parameter space in Eq.(3.1), but with the likelihood function  $\mathcal{L} = \mathcal{L}_{Higgs}$ . We find that the two sets of CRs overlap in broad regions. This fact reflects that the likelihood function for the DM sector does not contradict with that for the Higgs sector, and once the mass spectrum in the Higgs sector is determined, one can adjust the parameters in the sneutrino sector to be consistent with the measurements in DM physics.

### 3.3 DM annihilation mechanisms

In this subsection, we study the annihilation mechanisms of the CP-even sneutrino DM. For this purpose, we project the statistic quantities studied in Fig.3 on  $m_{A_1} - m_{\tilde{\nu}_1}$ ,  $m_{h_2} - m_{\tilde{\nu}_1}$  and  $\mu - m_{\tilde{\nu}_1}$  planes presented in Fig.4, and use the red dashed lines to denote the cases of  $m_{A_1} = m_{\tilde{\nu}_1}$ ,  $m_{h_2} = 2m_{\tilde{\nu}_1}$  and  $\mu = m_{\tilde{\nu}_1}$ , respectively. We also show in the last row of

Fig.4 the distribution of the mass splitting  $\Delta m$  on  $m_{\tilde{\nu}_{1,I}} - m_{\tilde{\nu}_1}$  plane, where we have split the plane into  $70 \times 70$  equal boxes (i.e. we divide each dimension of the plane by 70 equal bins), and defined  $\Delta m$  in each box as  $\Delta m \equiv \mathbf{min}(|m_{A_1} - m_{\tilde{\nu}_1} - m_{\tilde{\nu}_{1,I}}|)$  for the samples allocated in the box. Different CRs and IRs are also plotted for the left and right panel, respectively, with the red dashed lines corresponding to the case of  $m_{\tilde{\nu}_{1,I}} = m_{\tilde{\nu}_1}$ . From each row of panels in Fig.4, one can learn following facts:

- A large portion of samples satisfy  $m_{A_1} \lesssim m_{\tilde{\nu}_1}$ , which implies that the DM may annihilate dominantly into  $A_1 A_1$  final state. Since this annihilation channel is mainly a s-wave process,  $\langle \sigma v \rangle_0 \simeq \langle \sigma v \rangle_{FO} \simeq 3 \times 10^{-26} \text{cm}^3 \text{s}^{-1}$  with  $\langle \sigma v \rangle_0$  denoting current DM annihilation rate and  $\langle \sigma v \rangle_{FO}$  representing the rate at freeze-out temperature, and consequently the annihilation is tightly limited by the Fermi-LAT data from dwarf galaxies[94]. As was pointed in our work [45], such a constraint can be avoided by the forbidden annihilation proposed in [51] for  $m_{\tilde{\nu}_1} \lesssim 100 \text{GeV}$  or simply by requiring  $m_{\tilde{\nu}_1} > 100 \text{GeV}$  where the constraints become loose[94]. Our results verify this point. Note that for the case considered here, the sneutrino DM and the singlet-dominated  $A_1$  compose a self-contained DM sector, and this sector interacts with the SM sector only via the small Higgs-doublet component of  $A_1$ . This is a typical hidden or secluded DM scenario[95].
- Quite a few samples predict  $m_{h_2} \simeq 2m_{\tilde{\nu}_1}$ . In this case, the DM annihilation mainly proceeds via a s-channel resonant  $h_2$  funnel. Note that  $m_{h_2} > 2m_{\tilde{\nu}_1}$  for most samples in the  $1\sigma$  CR on the  $m_{h_2} - m_{\tilde{\nu}_1}$  plane, which implies  $\langle \sigma v \rangle_{FO} > \langle \sigma v \rangle_0$  if the  $h_2$ -mediated contribution is dominant in the annihilation[51].
- For most sample in the  $1\sigma$  CR on the  $\mu - m_{\tilde{\nu}_1}$  plane,  $\mu$  and  $m_{\tilde{\nu}_1}$  are approximately equal. In this case, the DM and Higgsinos can be in thermal equilibrium in early Universe before their freeze-out due to the transition between the DM pair and the Higgsino pair, which is mediated by the singlet-dominated Higgs bosons. As a result,  $\tilde{\nu}_1$  can reach the correct relic density by coannihilating with the Higgsino-dominated neutralinos, even when its couplings with the SM particles are tiny. This situation is quite similar to the sneutrino DM scenario in the inverse seesaw extension of the NMSSM[45].
- The lightest CP-odd sneutrino  $\tilde{\nu}_{1,I}$  may degenerate in mass with  $\tilde{\nu}_1$ . In this case,  $\tilde{\nu}_1$  can coannihilate with  $\tilde{\nu}_{1,I}$  to reach right relic density by exchanging the CP-odd scalar  $A_1$ . In particular, the relation  $m_{A_1} \simeq m_{\tilde{\nu}_1} + m_{\tilde{\nu}_{1,I}}$  may hold when  $55 \text{GeV} \leq \tilde{\nu}_1 \leq 190 \text{GeV}$ , which means that the coannihilation is mediated by a resonant  $A_1$ .

In summary, Fig.4 reveals the fact that the singlet dominated Higgs boson may either serve as the DM annihilation product, or mediate the DM annihilations in the Type-I extension of the NMSSM, and consequently, the lightest sneutrino in the theory can act as a viable DM candidate. This situation is quite different from the Type-I extension of the MSSM. Moreover, we remind that the  $\tilde{\nu}_1$ -Higgsino coannihilation was neglected in previous studies, but from our study it is actually the most important annihilation mechanism.

CP-even Sneutrino DM				CP-odd Sneutrino DM			
$\lambda$	0.12	$\kappa$	-0.20	$\lambda$	0.10	$\kappa$	0.23
$\tan\beta$	30.7	$\lambda_\nu$	0.20	$\tan\beta$	26.7	$\lambda_\nu$	0.05
$\mu$	145 GeV	$A_{\lambda_\nu}$	-221 GeV	$\mu$	252 GeV	$A_{\lambda_\nu}$	-405 GeV
$A_\kappa$	1.4 GeV	$A_t$	2807 GeV	$A_\kappa$	-2.1 GeV	$A_t$	2778 GeV
$m_\nu$	90 GeV	$m_{\tilde{\nu}_1}$	139 GeV	$m_\nu$	21 GeV	$m_{\tilde{\nu}_1}$	86 GeV
$m_{h_1}$	125.1 GeV	$m_{h_2}$	472 GeV	$m_{h_1}$	125.1 GeV	$m_{h_2}$	1190 GeV
$m_{h_3}$	2860 GeV	$m_{A_1}$	46.7 GeV	$m_{h_3}$	4223 GeV	$m_{A_1}$	32.5 GeV
$m_{A_2}$	2860 GeV	$m_{\tilde{\chi}_1^0}$	142.8 GeV	$m_{A_2}$	4223 GeV	$m_{\tilde{\chi}_1^0}$	248.1 GeV
$m_{\tilde{\chi}_2^0}$	154.3 GeV	$m_{\tilde{\chi}_1^\pm}$	149.1 GeV	$m_{\tilde{\chi}_2^0}$	263.8 GeV	$m_{\tilde{\chi}_1^\pm}$	257.2 GeV
$\sigma_{\tilde{\nu}_1-p}^{SI}$	$1.0 \times 10^{-46} \text{ cm}^2$	$\langle\sigma v\rangle_0$	$6.5 \times 10^{-26} \text{ cm}^3 \text{ s}^{-1}$	$\sigma_{\tilde{\nu}_1-p}^{SI}$	$1.0 \times 10^{-48} \text{ cm}^2$	$\langle\sigma v\rangle_0$	$2.0 \times 10^{-25} \text{ cm}^3 \text{ s}^{-1}$
$\Omega h^2$	0.118			$\Omega h^2$	0.119		

**Table 3.** Detailed information of the best point for the CP-even and CP-odd sneutrino DM cases.

### 3.4 DM-nucleon scattering

In Section 2, we have shown by analytic formulae the natural suppression of the cross section for  $\tilde{\nu}_1$ -nucleon scattering. In this subsection, we present relevant numerical results. In Fig.5, we plot the marginal posterior PDFs and PLs on  $\xi_2 - \xi_1$  planes (top panels) and  $\sigma_{\tilde{\nu}_1-p} - m_{\tilde{\nu}_1}$  planes (bottom panels). The top panels indicate that the typical magnitudes of  $\xi_i$  ( $i=1,2$ ) are  $10^{-11}\text{GeV}^{-3}$ , and both the CRs and CIs are not symmetric under the sign exchange of  $\xi_i$ . Correspondingly, the cross section for  $\tilde{\nu}_1$ -nucleon scattering is usually less than  $10^{-46}\text{cm}^2$ , and may be as low as  $10^{-49}\text{cm}^2$ , which are shown in the bottom panels.

From Eqs.(2.5,2.11) and the favored parameter space in Fig.1, one can learn that the scattering rate is sensitive to the parameters  $\lambda_\nu$  and  $A_{\lambda_\nu}$ , so we concentrate on these two parameters in following discussion. In the upper panels of Fig.6, we show the dependence of posterior PDF and PL on them, and in the lower panels we plot the distribution of the fine tuning parameter  $\Delta_{FT}$  defined in Eq.(2.12). The upper panels indicate that both the  $1\sigma$  posterior PDF and  $1\sigma$  PL spread a broad region on the plane, reflecting that the theory can readily accommodate the tight constraints from the XENON1T-2018 experiments. The lower panels, on the other hand, show that the theory does not need any fine tuning to survive the tight constraints.

In a similar way, one may discuss the results for the CP-odd sneutrino DM case. We find that the Bayesian evidence for the CP-odd case is  $\ln Z = -48.1$ , which is significantly smaller than  $\ln Z = -47.7$  for the CP-even DM case. We also find that the  $\chi^2$ s of the best points for the two cases are roughly equal,  $\chi_{min}^2 \simeq 37.3$ , with most of its contribution coming from the Higgs sector, which contains 74 observables in the peak-centered method of the package HiggsSignal[82]. Since the underlying physics of the two cases are same, we do not carry out a detailed analysis anymore, instead we present the 1D posterior PDFs and PLs in the right panels of Fig.1 and Fig.2 in comparison with the results of the CP-even

DM case, and the 2D results in Fig.7-10, which are analogy with Fig.3-6 for the CP-even DM case. We also show the detailed information of the best fit points for the two cases in Table 3.

#### 4 Constraints from the LHC experiments

In supersymmetric theories, moderately light Higgsinos are favored by naturalness. So the Higgsinos are expected to be copiously produced at the LHC, and the detection of their signals can significantly limit the theory[34, 64, 96]. In the NMSSM with Type-I seesaw mechanism, the neutral Higgsinos mix with the Singlino, the fermionic component field of the singlet superfield  $\hat{S}$ , to form mass eigenstates called neutralinos. Due to the tininess of the Yukawa coupling  $Y_\nu$ , the Higgsino-dominated neutralinos may have a much stronger coupling with the  $\tilde{\nu}_{R,I}\nu_R$  state, which is induced by the  $\lambda_\nu\hat{S}\hat{\nu}\hat{\nu}$  term in the superpotential, than with the  $\tilde{\nu}_{R,I}\nu_L$  state, which comes from the  $Y_\nu\hat{l}\cdot\hat{H}_u\hat{\nu}$  interaction. The decay product of the neutralinos is then complicated by the decay chain  $\tilde{\chi}^0 \rightarrow \tilde{\nu}_{R,I}\nu_R$  with  $\nu_R \rightarrow W^{(*)}l, Z^{(*)}\nu_L, h^{(*)}\nu_L$ [97]<sup>7</sup>. On the other hand, this situation is simplified greatly for the Higgsino-dominated chargino, which may decay only by the channel  $\tilde{\chi}^\pm \rightarrow \tilde{\nu}_{R,I}\tau^\pm$  if  $\tilde{\nu}_{R,I}$  carry  $\tau$  flavor. So in this subsection we investigate the constraints of the ATLAS analysis at 8-TeV LHC on the signal of two hadronic  $\tau$ s plus  $E_T^{miss}$ [98], which arises from the process  $pp \rightarrow \tilde{\chi}_1^\pm\tilde{\chi}_1^\mp \rightarrow 2\tau + E_T^{miss}$  in the Type-I extension.

In our calculation, we use the simulation tools MadGraph/MadEvent[99, 100] to generate the parton level events of the processes, Pythia6[101] for parton fragmentation and hadronization, Delphes[102] for fast simulation of the performance of the ATLAS detector, and CheckMATE[103–105] to implement the cut selections of the analysis. The validation on the implementation of the analysis in CheckMATE was provided in our work[45].

The procedure to get the constraints is as follows: we first determine the signal region (SR) with the largest expected sensitivity for a given parameter point  $(m_{\tilde{\nu}_1}, m_{\tilde{\chi}_1^\pm})$  (see footnote 6 in [45] for more details), then we calculate its  $R$  value defined by  $R \equiv S/S_{95}^{OBS}$ , where  $S$  stands for the number of signal events in the SR with the statistical uncertainty considered and  $S_{95}^{OBS}$  denotes the observed limit at 95% confidence level for the SR. Obviously,  $R$  represents the capability of the LHC in exploring the point.  $R > 1$  implies that the point is excluded, or else it is allowed. In Fig.11, we present our results of  $R$  as a function of  $m_{\tilde{\nu}_1}$  for four choices of  $m_{\tilde{\chi}_1^\pm}, m_{\tilde{\chi}_1^\pm} = 120\text{GeV}, 160\text{GeV}, 200\text{GeV}, 240\text{GeV}$ . This figure indicates that  $R$  increases monotonously with the enlarged mass splitting  $\Delta m \equiv m_{\tilde{\chi}_1^\pm} - m_{\tilde{\nu}_1}$  for fixed  $m_{\tilde{\chi}_1^\pm}$ , and  $R = 1$  corresponds to  $\Delta m = 65\text{GeV}, 70\text{GeV}, 85\text{GeV}, 150\text{GeV}$ , respectively, for the  $m_{\tilde{\chi}_1^\pm}$ s<sup>8</sup>. The underlying physics is that a large mass splitting tends to enhance the cut

<sup>7</sup>In our discussion, we assume that sparticles other than  $\tilde{\nu}_{R,I}$  are much heavier than the Higgsinos. If the decay  $\tilde{\chi}^0 \rightarrow \tilde{\nu}_{R,I}\nu_R$  is kinematically forbidden,  $\tilde{\chi}^0$  has to decay into  $\tilde{\nu}_{R,I}\nu_L$  assuming no mass splitting among the Higgsino-dominated particles. In this case, the experimental constraints on the Mono-jet signal from the neutralino pair production is rather weak, which has been shown in our previous work [45].

<sup>8</sup>We note that recently both the ATLAS and CMS collaboration updated their analysis on the  $2\tau + E_T^{miss}$  signal[107–110]. By private discussion with Dr. Y. Zhang and P.X. Zhu who are working on the new analyses for CheckMATE collaboration, we learn that  $R = 1$  corresponds to  $\Delta m \simeq 75\text{GeV}, 90\text{GeV}, 110\text{GeV}, 125\text{GeV}$ ,

efficiency, and the number of the signal event  $S$  depends on both the cut efficiency and the production rate  $\sigma(pp \rightarrow \tilde{\chi}_1^\pm \tilde{\chi}_1^\mp)$ , which decreases as the chargino becomes heavy[106].

With respect to the results in Fig.11, two points should be noted. One is that we have assumed  $Br(\tilde{\chi}_1^\pm \rightarrow \tilde{\nu}_1 \tau) = 100\%$  in getting the figure. But in practice,  $\tilde{\nu}_1$  may be either  $\tilde{\nu}_{1,R}$  or  $\tilde{\nu}_{1,I}$ , and the two channels  $\tilde{\chi}_1^\pm \rightarrow \tilde{\nu}_{1,R}\tau, \tilde{\nu}_{1,I}\tau$  can be kinematically accessible simultaneously. Moreover, the chargino may decay first into  $\tilde{\chi}_1^0 jj'/\pi^\pm$  after considering the mass splitting among the Higgsino-dominated particles[64]. So in case of  $Br(\tilde{\chi}_1^\pm \rightarrow \tilde{\nu}_1 \tau) < 1$ , the  $R$  value in Fig.11 should be rescaled by the factor of  $Br^2(\tilde{\chi}_1^\pm \rightarrow \tilde{\nu}_1 \tau)$ , which can weaken the constraint. The other is that, from the plots on the  $\mu - \tilde{\nu}_1$  plane in Fig.4 and 8, the mass splitting  $\Delta m$  is of  $\mathcal{O}(10\text{GeV})$  for most samples. In this case, the LHC searches for the  $2\tau$  signal actually have no exclusion ability.

## 5 Conclusions

Given the strong tension between the naturalness for  $Z$  boson mass and the DD experiments for customary neutralino DM candidate in minimal supersymmetric theories, it is essential to explore the DM physics in any extension of the MSSM or the NMSSM. In this work, we augment the NMSSM with Type-I seesaw mechanism, which is the simplest extension to reconcile the neutrino non-zero masses and neutrinos oscillation experiment, and carry out a comprehensive study on sneutrino DM scenarios. The highlight of the theory is that the singlet Higgs field plays an important role in various aspects, including generating the Higgsino mass and the heavy neutrino masses dynamically, mediating the transition between the DM pair and Higgsino pair to keep them in thermal bath in early Universe, acting as DM annihilation final state or mediating DM annihilations, as well as contributing to DM-nucleon scattering rate. As a result, the scattering of the sneutrino DM with nucleon can be suppressed in a natural way and by several mechanisms so that the tension is alleviated greatly even after considering the latest XENON1T results. In order to illustrate these features, we carry out a sophisticated scan over the vast parameter space by Nested Sampling method, and adopt both Bayesian and frequentist statistical quantities to analyze the favored parameter space of the scenarios, the DM annihilation mechanism as well as the behavior of the DM-nucleon scattering confronted with the tight DD constraints. For the sake of the statistical inference, we construct the likelihood function by considering B-physics measurements, Higgs data, DM relic density as well as DM direct detection and indirect detection limits. We obtain following key conclusions:

- (1) The model provides a viable sneutrino DM candidate over broad parameter regions. In particular, moderately light Higgsinos,  $\mu \lesssim 240\text{GeV}$ , are favored by the DM physics, which may be viewed as an another advantage of the theory. To the best of our knowledge, the model may be the minimal framework to accommodate a realistic sneutrino DM candidate.

---

respectively, for the most optimized SR of the analyses at 13TeV-LHC. The results in comparison with those in Fig.11 reflect that the analyses at the 13TeV-LHC are more powerful in limiting the model than that at the 8TeV-LHC only when  $m_{\tilde{\chi}_1^\pm} \gtrsim 220\text{GeV}$  since the updated analyses focus on heavy Chargino case, which requires more energetic jets and larger missing energy than the original analysis.

- (2) The DM and the singlet-dominated Higgs bosons can compose a realistic DM sector, which communicates with the SM sector only by the small doublet component in the bosons. This is a typical feature of hidden or secluded DM scenario.
- (3) In most cases, the DM co-annihilated with the Higgsinos to get the right relic density, which was omitted in previous studies.
- (4) The sneutrino DM scenarios satisfy the tight constraints from the recent XENON1T experiment on DM-nucleon scattering without any fine tuning.
- (5) The sneutrino DM scenarios can easily survive the constraints from the direct searches for electroweakinos with the final states of  $2\tau + E_{miss}^T$  signal at the LHC.

Finally, we mention that, although we have optimized our computer codes for the calculation, it is still time-consuming (about 30000 hours for a single core in Intel I9 7900X CPU) to finish the scan. This is challenging for our computer cluster. We also mention that the conclusions listed above may be applied to the inverse seesaw extension of the NMSSM due to the similarities of the two frameworks, and a careful study of the model is necessary.

## Acknowledgement

We thank Dr. Yangle He, Yang Zhang and Pengxuan Zhu for helpful discussion about dark matter indirect detection experiments. This work is supported by the National Natural Science Foundation of China (NNSFC) under grant No. 11575053.

## References

- [1] P. A. R. Ade *et al.* [Planck Collaboration], *Astron. Astrophys.* **594**, A13 (2016) doi:10.1051/0004-6361/201525830 [arXiv:1502.01589 [astro-ph.CO]].
- [2] G. Bertone and D. Hooper, [arXiv:1605.04909 [astro-ph.CO]].
- [3] F. Iocco, M. Pato and G. Bertone, *Nature Phys.* **11**, 245 (2015) doi:10.1038/nphys3237 [arXiv:1502.03821 [astro-ph.GA]].
- [4] V. Springel, C. S. Frenk and S. D. M. White, *Nature* **440**, 1137 (2006) doi:10.1038/nature04805 [astro-ph/0604561].
- [5] G. Bertone, D. Hooper and J. Silk, *Phys. Rept.* **405**, 279 (2005) doi:10.1016/j.physrep.2004.08.031 [hep-ph/0404175].
- [6] G. Arcadi, M. Dutra, P. Ghosh, M. Lindner, Y. Mambrini, M. Pierre, S. Profumo and F. S. Queiroz, arXiv:1703.07364 [hep-ph].
- [7] R. K. Leane, T. R. Slatyer, J. F. Beacom and K. C. Y. Ng, arXiv:1805.10305 [hep-ph].
- [8] J. S. Hagelin, G. L. Kane and S. Raby, *Nucl. Phys. B* **241**, 638 (1984). doi:10.1016/0550-3213(84)90064-6
- [9] G. Jungman, M. Kamionkowski and K. Griest, *Phys. Rept.* **267**, 195 (1996) doi:10.1016/0370-1573(95)00058-5 [hep-ph/9506380].

- [10] C. Arina and N. Fornengo, JHEP **0711**, 029 (2007) doi:10.1088/1126-6708/2007/11/029 [arXiv:0709.4477 [hep-ph]].
- [11] A. Tan *et al.* [PandaX-II Collaboration], Phys. Rev. Lett. **117**, no. 12, 121303 (2016) doi:10.1103/PhysRevLett.117.121303 [arXiv:1607.07400 [hep-ex]].
- [12] C. Fu *et al.* [PandaX-II Collaboration], Phys. Rev. Lett. **118**, no. 7, 071301 (2017) Erratum: [Phys. Rev. Lett. **120**, no. 4, 049902 (2018)] doi:10.1103/PhysRevLett.120.049902, 10.1103/PhysRevLett.118.071301 [arXiv:1611.06553 [hep-ex]].
- [13] D. S. Akerib *et al.* [LUX Collaboration], Phys. Rev. Lett. **118**, no. 2, 021303 (2017) doi:10.1103/PhysRevLett.118.021303 [arXiv:1608.07648 [astro-ph.CO]].
- [14] E. Aprile *et al.* [XENON Collaboration], Phys. Rev. Lett. **119**, no. 18, 181301 (2017) doi:10.1103/PhysRevLett.119.181301 [arXiv:1705.06655 [astro-ph.CO]].
- [15] E. Aprile *et al.* [XENON Collaboration], arXiv:1805.12562 [astro-ph.CO].
- [16] H. Baer, V. Barger and H. Serce, Phys. Rev. D **94**, no. 11, 115019 (2016) doi:10.1103/PhysRevD.94.115019 [arXiv:1609.06735 [hep-ph]].
- [17] P. Huang, R. A. Roglans, D. D. Spiegel, Y. Sun and C. E. M. Wagner, Phys. Rev. D **95**, no. 9, 095021 (2017) doi:10.1103/PhysRevD.95.095021 [arXiv:1701.02737 [hep-ph]].
- [18] M. Badziak, M. Olechowski and P. Szczerbiak, Phys. Lett. B **770**, 226 (2017) doi:10.1016/j.physletb.2017.04.059 [arXiv:1701.05869 [hep-ph]].
- [19] R. N. Mohapatra *et al.*, Rept. Prog. Phys. **70**, 1757 (2007) doi:10.1088/0034-4885/70/11/R02 [hep-ph/0510213].
- [20] P. Minkowski, Phys. Lett. **67B** (1977) 421. doi:10.1016/0370-2693(77)90435-X
- [21] J. Schechter and J. W. F. Valle, Phys. Rev. D **22**, 2227 (1980). doi:10.1103/PhysRevD.22.2227
- [22] R. Foot, H. Lew, X. G. He and G. C. Joshi, Z. Phys. C **44**, 441 (1989). doi:10.1007/BF01415558
- [23] R. N. Mohapatra, Phys. Rev. Lett. **56**, 561 (1986). doi:10.1103/PhysRevLett.56.561
- [24] R. N. Mohapatra and J. W. F. Valle, Phys. Rev. D **34**, 1642 (1986). doi:10.1103/PhysRevD.34.1642
- [25] T. Asaka, K. Ishiwata and T. Moroi, Phys. Rev. D **73**, 051301 (2006) doi:10.1103/PhysRevD.73.051301 [hep-ph/0512118]. T. Asaka, K. Ishiwata and T. Moroi, Phys. Rev. D **75**, 065001 (2007) doi:10.1103/PhysRevD.75.065001 [hep-ph/0612211].
- [26] S. Gopalakrishna, A. de Gouvea and W. Porod, JCAP **0605**, 005 (2006) doi:10.1088/1475-7516/2006/05/005 [hep-ph/0602027].
- [27] J. McDonald, JCAP **0701**, 001 (2007) doi:10.1088/1475-7516/2007/01/001 [hep-ph/0609126].
- [28] H. S. Lee, K. T. Matchev and S. Nasri, Phys. Rev. D **76**, 041302 (2007) doi:10.1103/PhysRevD.76.041302 [hep-ph/0702223 [HEP-PH]].
- [29] N. Arkani-Hamed, L. J. Hall, H. Murayama, D. Tucker-Smith and N. Weiner, Phys. Rev. D **64**, 115011 (2001) doi:10.1103/PhysRevD.64.115011 [hep-ph/0006312].
- [30] D. Hooper, J. March-Russell and S. M. West, Phys. Lett. B **605**, 228 (2005) doi:10.1016/j.physletb.2004.11.047 [hep-ph/0410114].

- [31] Z. Thomas, D. Tucker-Smith and N. Weiner, *Phys. Rev. D* **77**, 115015 (2008) doi:10.1103/PhysRevD.77.115015 [arXiv:0712.4146 [hep-ph]].
- [32] G. Belanger, M. Kakizaki, E. K. Park, S. Kraml and A. Pukhov, *JCAP* **1011**, 017 (2010) doi:10.1088/1475-7516/2010/11/017 [arXiv:1008.0580 [hep-ph]].
- [33] B. Dumont, G. Belanger, S. Fichet, S. Kraml and T. Schwetz, *JCAP* **1209**, 013 (2012) doi:10.1088/1475-7516/2012/09/013 [arXiv:1206.1521 [hep-ph]].
- [34] C. Arina and M. E. Cabrera, *JHEP* **1404**, 100 (2014) doi:10.1007/JHEP04(2014)100 [arXiv:1311.6549 [hep-ph]].
- [35] U. Ellwanger, C. Hugonie and A. M. Teixeira, *Phys. Rept.* **496**, 1 (2010) doi:10.1016/j.physrep.2010.07.001 [arXiv:0910.1785 [hep-ph]].
- [36] L. J. Hall, D. Pinner and J. T. Ruderman, *JHEP* **1204**, 131 (2012) doi:10.1007/JHEP04(2012)131 [arXiv:1112.2703 [hep-ph]].
- [37] U. Ellwanger, *JHEP* **1203**, 044 (2012) doi:10.1007/JHEP03(2012)044 [arXiv:1112.3548 [hep-ph]].
- [38] J. J. Cao, Z. X. Heng, J. M. Yang, Y. M. Zhang and J. Y. Zhu, *JHEP* **1203**, 086 (2012) doi:10.1007/JHEP03(2012)086 [arXiv:1202.5821 [hep-ph]].
- [39] J. Cao, F. Ding, C. Han, J. M. Yang and J. Zhu, *JHEP* **1311**, 018 (2013) doi:10.1007/JHEP11(2013)018 [arXiv:1309.4939 [hep-ph]].
- [40] U. Ellwanger and A. M. Teixeira, *JHEP* **1410**, 113 (2014) doi:10.1007/JHEP10(2014)113 [arXiv:1406.7221 [hep-ph]].
- [41] J. Cao, L. Shang, P. Wu, J. M. Yang and Y. Zhang, *Phys. Rev. D* **91**, no. 5, 055005 (2015) doi:10.1103/PhysRevD.91.055005 [arXiv:1410.3239 [hep-ph]].
- [42] J. Cao, L. Shang, P. Wu, J. M. Yang and Y. Zhang, *JHEP* **1510**, 030 (2015) doi:10.1007/JHEP10(2015)030 [arXiv:1506.06471 [hep-ph]].
- [43] J. Cao, Y. He, L. Shang, W. Su and Y. Zhang, *JHEP* **1608**, 037 (2016) doi:10.1007/JHEP08(2016)037 [arXiv:1606.04416 [hep-ph]].
- [44] U. Ellwanger and C. Hugonie, arXiv:1806.09478 [hep-ph].
- [45] J. Cao, X. Guo, Y. He, L. Shang and Y. Yue, *JHEP* **1710**, 044 (2017) doi:10.1007/JHEP10(2017)044 [arXiv:1707.09626 [hep-ph]].
- [46] J. Chang, K. Cheung, H. Ishida, C. T. Lu, M. Spinrath and Y. L. S. Tsai, *JHEP* **1710**, 039 (2017) doi:10.1007/JHEP10(2017)039 [arXiv:1707.04374 [hep-ph]].
- [47] J. Chang, K. Cheung, H. Ishida, C. T. Lu, M. Spinrath and Y. L. S. Tsai, arXiv:1806.04468 [hep-ph].
- [48] J. Cao, Y. He, L. Shang, W. Su, P. Wu and Y. Zhang, *JHEP* **1610**, 136 (2016) doi:10.1007/JHEP10(2016)136 [arXiv:1609.00204 [hep-ph]].
- [49] F. Feroz, M. P. Hobson and M. Bridges, *Mon. Not. Roy. Astron. Soc.* **398**, 1601 (2009) doi:10.1111/j.1365-2966.2009.14548.x [arXiv:0809.3437 [astro-ph]].
- [50] M. J. Baker *et al.*, *JHEP* **1512**, 120 (2015) doi:10.1007/JHEP12(2015)120 [arXiv:1510.03434 [hep-ph]].
- [51] K. Griest and D. Seckel, *Phys. Rev. D* **43**, 3191 (1991). doi:10.1103/PhysRevD.43.3191

- [52] R. Kitano and K. y. Oda, Phys. Rev. D **61**, 113001 (2000) doi:10.1103/PhysRevD.61.113001 [hep-ph/9911327].
- [53] D. G. Cerdeno, C. Munoz and O. Seto, Phys. Rev. D **79**, 023510 (2009) doi:10.1103/PhysRevD.79.023510 [arXiv:0807.3029 [hep-ph]].
- [54] D. G. Cerdeno and O. Seto, JCAP **0908**, 032 (2009) doi:10.1088/1475-7516/2009/08/032 [arXiv:0903.4677 [hep-ph]].
- [55] D. G. Cerdeno, J. H. Huh, M. Peiro and O. Seto, JCAP **1111**, 027 (2011) doi:10.1088/1475-7516/2011/11/027 [arXiv:1108.0978 [hep-ph]].
- [56] W. Wang, J. M. Yang and L. L. You, JHEP **1307**, 158 (2013) doi:10.1007/JHEP07(2013)158 [arXiv:1303.6465 [hep-ph]].
- [57] A. Chatterjee, D. Das, B. Mukhopadhyaya and S. K. Rai, JCAP **1407**, 023 (2014) doi:10.1088/1475-7516/2014/07/023 [arXiv:1401.2527 [hep-ph]].
- [58] D. G. Cerdeño, M. Peir and S. Robles, JCAP **1408**, 005 (2014) doi:10.1088/1475-7516/2014/08/005 [arXiv:1404.2572 [hep-ph]].
- [59] K. Huitu and H. Waltari, JHEP **1411**, 053 (2014) doi:10.1007/JHEP11(2014)053 [arXiv:1405.5330 [hep-ph]].
- [60] Y. L. Tang, Nucl. Phys. B **890**, 263 (2014) doi:10.1016/j.nuclphysb.2014.11.012 [arXiv:1411.1892 [hep-ph]].
- [61] D. G. Cerdeno, M. Peiro and S. Robles, Phys. Rev. D **91**, no. 12, 123530 (2015) doi:10.1103/PhysRevD.91.123530 [arXiv:1501.01296 [hep-ph]].
- [62] T. Gherghetta, B. von Harling, A. D. Medina, M. A. Schmidt and T. Trott, Phys. Rev. D **91**, 105004 (2015) doi:10.1103/PhysRevD.91.105004 [arXiv:1502.07173 [hep-ph]].
- [63] D. G. Cerdeño, V. De Romeri, V. Martn-Lozano, K. A. Olive and O. Seto, Eur. Phys. J. C **78**, no. 4, 290 (2018) doi:10.1140/epjc/s10052-018-5689-0 [arXiv:1707.03990 [hep-ph]].
- [64] A. Chatterjee, J. Dutta and S. K. Rai, JHEP **1806**, 042 (2018) doi:10.1007/JHEP06(2018)042 [arXiv:1710.10617 [hep-ph]].
- [65] E. Bagnaschi *et al.*, Eur. Phys. J. C **78**, no. 3, 256 (2018) doi:10.1140/epjc/s10052-018-5697-0 [arXiv:1710.11091 [hep-ph]].
- [66] G. Belanger, F. Boudjema, A. Pukhov and A. Semenov, Comput. Phys. Commun. **185**, 960 (2014) doi:10.1016/j.cpc.2013.10.016 [arXiv:1305.0237 [hep-ph]].
- [67] T. Han and R. Hempfling, Phys. Lett. B **415**, 161 (1997) doi:10.1016/S0370-2693(97)01205-7 [hep-ph/9708264].
- [68] J. M. Alarcon, J. Martin Camalich and J. A. Oller, Phys. Rev. D **85**, 051503 (2012) doi:10.1103/PhysRevD.85.051503 [arXiv:1110.3797 [hep-ph]].
- [69] J. M. Alarcon, L. S. Geng, J. Martin Camalich and J. A. Oller, Phys. Lett. B **730**, 342 (2014) doi:10.1016/j.physletb.2014.01.065 [arXiv:1209.2870 [hep-ph]].
- [70] D. Barducci, G. Belanger, J. Bernon, F. Boudjema, J. Da Silva, S. Kraml, U. Laa and A. Pukhov, arXiv:1606.03834 [hep-ph].
- [71] G. Belanger, F. Boudjema, C. Hugonie, A. Pukhov and A. Semenov, JCAP **0509**, 001 (2005) doi:10.1088/1475-7516/2005/09/001 [hep-ph/0505142].

- [72] A. Crivellin, M. Hoferichter, M. Procura and L. C. Tunstall, *JHEP* **1507**, 129 (2015) doi:10.1007/JHEP07(2015)129 [arXiv:1503.03478 [hep-ph]].
- [73] M. Badziak, M. Olechowski and P. Szczerbiak, *JHEP* **1603**, 179 (2016) doi:10.1007/JHEP03(2016)179 [arXiv:1512.02472 [hep-ph]].
- [74] T. Han, F. Kling, S. Su and Y. Wu, *JHEP* **1702**, 057 (2017) doi:10.1007/JHEP02(2017)057 [arXiv:1612.02387 [hep-ph]].
- [75] M. Badziak, M. Olechowski and P. Szczerbiak, arXiv:1705.00227 [hep-ph].
- [76] F. Staub, *Comput. Phys. Commun.* **185**, 1773 (2014) doi:10.1016/j.cpc.2014.02.018 [arXiv:1309.7223 [hep-ph]].
- [77] F. Staub, *Comput. Phys. Commun.* **184**, 1792 (2013) doi:10.1016/j.cpc.2013.02.019 [arXiv:1207.0906 [hep-ph]].
- [78] F. Staub, arXiv:0806.0538 [hep-ph].
- [79] W. Porod and F. Staub, *Comput. Phys. Commun.* **183**, 2458 (2012) doi:10.1016/j.cpc.2012.05.021 [arXiv:1104.1573 [hep-ph]].
- [80] W. Porod, F. Staub and A. Vicente, *Eur. Phys. J. C* **74**, no. 8, 2992 (2014) doi:10.1140/epjc/s10052-014-2992-2 [arXiv:1405.1434 [hep-ph]].
- [81] P. Bechtle, S. Heinemeyer, O. Stal, T. Stefaniak and G. Weiglein, *Eur. Phys. J. C* **75**, no. 9, 421 (2015) doi:10.1140/epjc/s10052-015-3650-z [arXiv:1507.06706 [hep-ph]].
- [82] P. Bechtle, S. Heinemeyer, O. Stal, T. Stefaniak and G. Weiglein, *JHEP* **1411**, 039 (2014) doi:10.1007/JHEP11(2014)039 [arXiv:1403.1582 [hep-ph]].
- [83] J. h. Park, *Phys. Rev. D* **83**, 055015 (2011) doi:10.1103/PhysRevD.83.055015 [arXiv:1011.4939 [hep-ph]].
- [84] D. Chowdhury, R. M. Godbole, K. A. Mohan and S. K. Vempati, *JHEP* **1402**, 110 (2014) Erratum: [*JHEP* **1803**, 149 (2018)] doi:10.1007/JHEP03(2018)149, 10.1007/JHEP02(2014)110 [arXiv:1310.1932 [hep-ph]].
- [85] EasyScan\_HEP, <http://easyscanhep.hepforge.org>.
- [86] P. Gregory, *Bayesian Logical Data Analysis for the Physical Sciences*. Cambridge University Press, 2005.
- [87] P. Athron, C. Balazs, B. Farmer, A. Fowlie, D. Harries and D. Kim, *JHEP* **1710**, 160 (2017) doi:10.1007/JHEP10(2017)160 [arXiv:1709.07895 [hep-ph]].
- [88] S. Matsumoto, S. Mukhopadhyay and Y. L. S. Tsai, *Phys. Rev. D* **94** (2016) no.6, 065034 doi:10.1103/PhysRevD.94.065034 [arXiv:1604.02230 [hep-ph]].
- [89] see website: [www-glast.stanford.edu/pub\\_data/1048](http://www-glast.stanford.edu/pub_data/1048)
- [90] L. M. Carpenter, R. Colburn, J. Goodman and T. Linden, *Phys. Rev. D* **94**, no. 5, 055027 (2016) doi:10.1103/PhysRevD.94.055027 [arXiv:1606.04138 [hep-ph]].
- [91] X. J. Huang, C. C. Wei, Y. L. Wu, W. H. Zhang and Y. F. Zhou, *Phys. Rev. D* **95**, no. 6, 063021 (2017) doi:10.1103/PhysRevD.95.063021 [arXiv:1611.01983 [hep-ph]].
- [92] S. Li *et al.*, arXiv:1806.00733 [astro-ph.HE].
- [93] A. Fowlie and M. H. Bardsley, *Eur. Phys. J. Plus* **131**, no. 11, 391 (2016) doi:10.1140/epjp/i2016-16391-0 [arXiv:1603.00555 [physics.data-an]].

- [94] M. Ackermann *et al.* [Fermi-LAT Collaboration], Phys. Rev. Lett. **115**, no. 23, 231301 (2015) doi:10.1103/PhysRevLett.115.231301 [arXiv:1503.02641 [astro-ph.HE]].
- [95] M. Pospelov, A. Ritz and M. B. Voloshin, Phys. Lett. B **662**, 53 (2008) doi:10.1016/j.physletb.2008.02.052 [arXiv:0711.4866 [hep-ph]].
- [96] J. Guo, Z. Kang, J. Li, T. Li and Y. Liu, JHEP **1410**, 164 (2014) doi:10.1007/JHEP10(2014)164 [arXiv:1312.2821 [hep-ph]].
- [97] D. G. Cerdeno, V. Martin-Lozano and O. Seto, JHEP **1405**, 035 (2014) doi:10.1007/JHEP05(2014)035 [arXiv:1311.7260 [hep-ph]].
- [98] G. Aad *et al.* [ATLAS Collaboration], JHEP **1410**, 096 (2014) doi:10.1007/JHEP10(2014)096 [arXiv:1407.0350 [hep-ex]].
- [99] J. Alwall *et al.*, JHEP **1407**, 079 (2014) doi:10.1007/JHEP07(2014)079 [arXiv:1405.0301 [hep-ph]].
- [100] J. Alwall, M. Herquet, F. Maltoni, O. Mattelaer and T. Stelzer, JHEP **1106**, 128 (2011) doi:10.1007/JHEP06(2011)128 [arXiv:1106.0522 [hep-ph]].
- [101] T. Sjostrand, S. Mrenna and P. Z. Skands, JHEP **0605**, 026 (2006) doi:10.1088/1126-6708/2006/05/026 [hep-ph/0603175].
- [102] J. de Favereau *et al.* [DELPHES 3 Collaboration], JHEP **1402**, 057 (2014) doi:10.1007/JHEP02(2014)057 [arXiv:1307.6346 [hep-ex]].
- [103] D. Dercks, N. Desai, J. S. Kim, K. Rolbiecki, J. Tattersall and T. Weber, arXiv:1611.09856 [hep-ph].
- [104] J. S. Kim, D. Schmeier, J. Tattersall and K. Rolbiecki, Comput. Phys. Commun. **196**, 535 (2015) doi:10.1016/j.cpc.2015.06.002 [arXiv:1503.01123 [hep-ph]].
- [105] M. Drees, H. Dreiner, D. Schmeier, J. Tattersall and J. S. Kim, Comput. Phys. Commun. **187**, 227 (2015) doi:10.1016/j.cpc.2014.10.018 [arXiv:1312.2591 [hep-ph]].
- [106] W. Beenakker, R. Hopker and M. Spira, hep-ph/9611232.
- [107] CMS Collaboration [CMS Collaboration], missing transverse momentum in proton-proton collisions at sqrt(s)=13 TeV,” CMS-PAS-SUS-17-002.
- [108] CMS Collaboration [CMS Collaboration], CMS-PAS-SUS-17-003.
- [109] A. M. Sirunyan *et al.* [CMS Collaboration], [arXiv:1806.05264 [hep-ex]].
- [110] M. Aaboud *et al.* [ATLAS Collaboration], Eur. Phys. J. C **78**, no. 2, 154 (2018) doi:10.1140/epjc/s10052-018-5583-9 [arXiv:1708.07875 [hep-ex]].

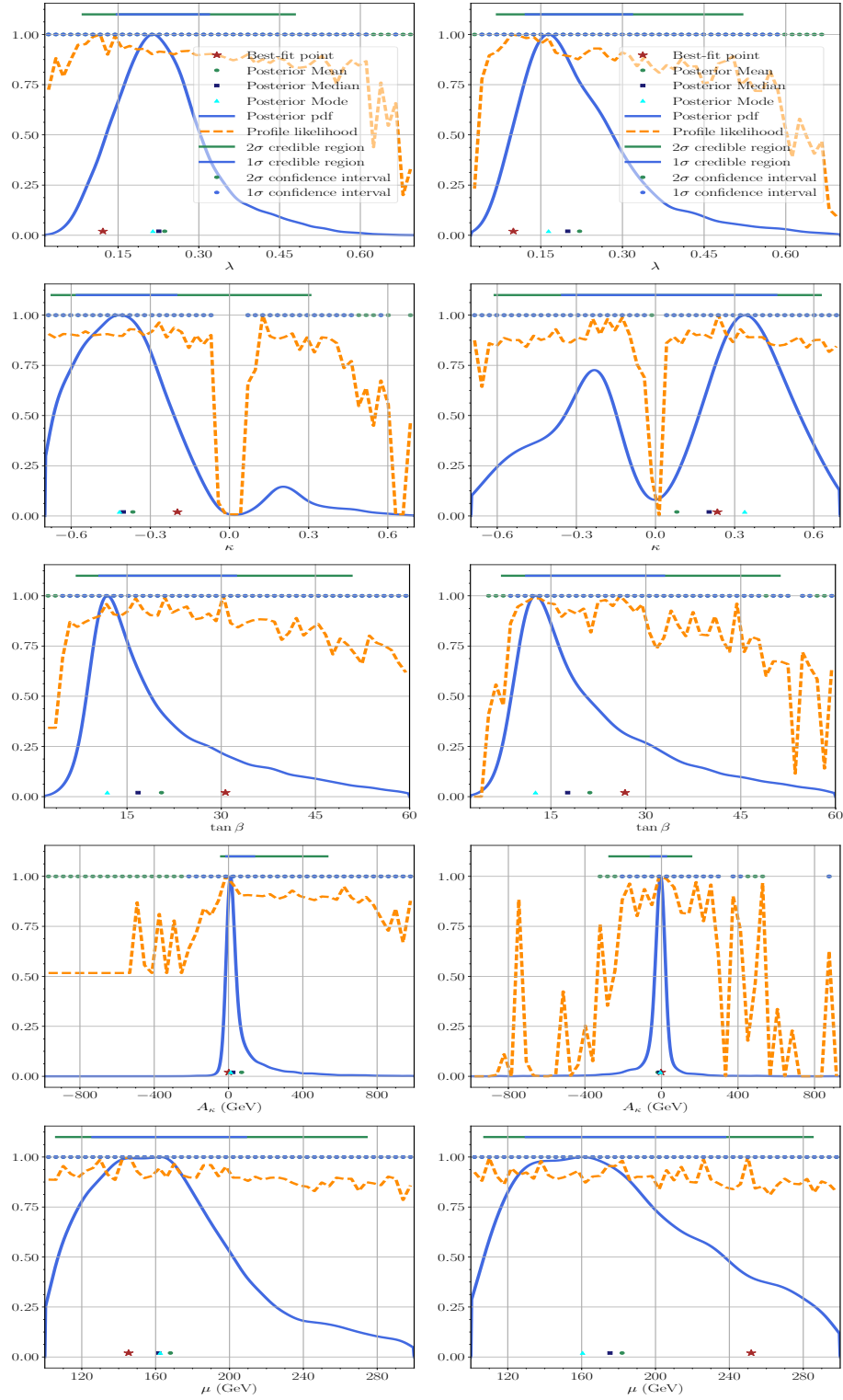


**Figure 1.** **Left panels:** One-dimensional marginal posterior PDFs and PLs as a function of  $\lambda$ ,  $\kappa$ ,  $\tan\beta$ ,  $A_\kappa$  and  $\mu$ , respectively. Credible regions, confidence intervals and other statistic quantities are also presented. **Right panels:** Same as the left panels, but for the case that the sneutrino DM is CP-odd.

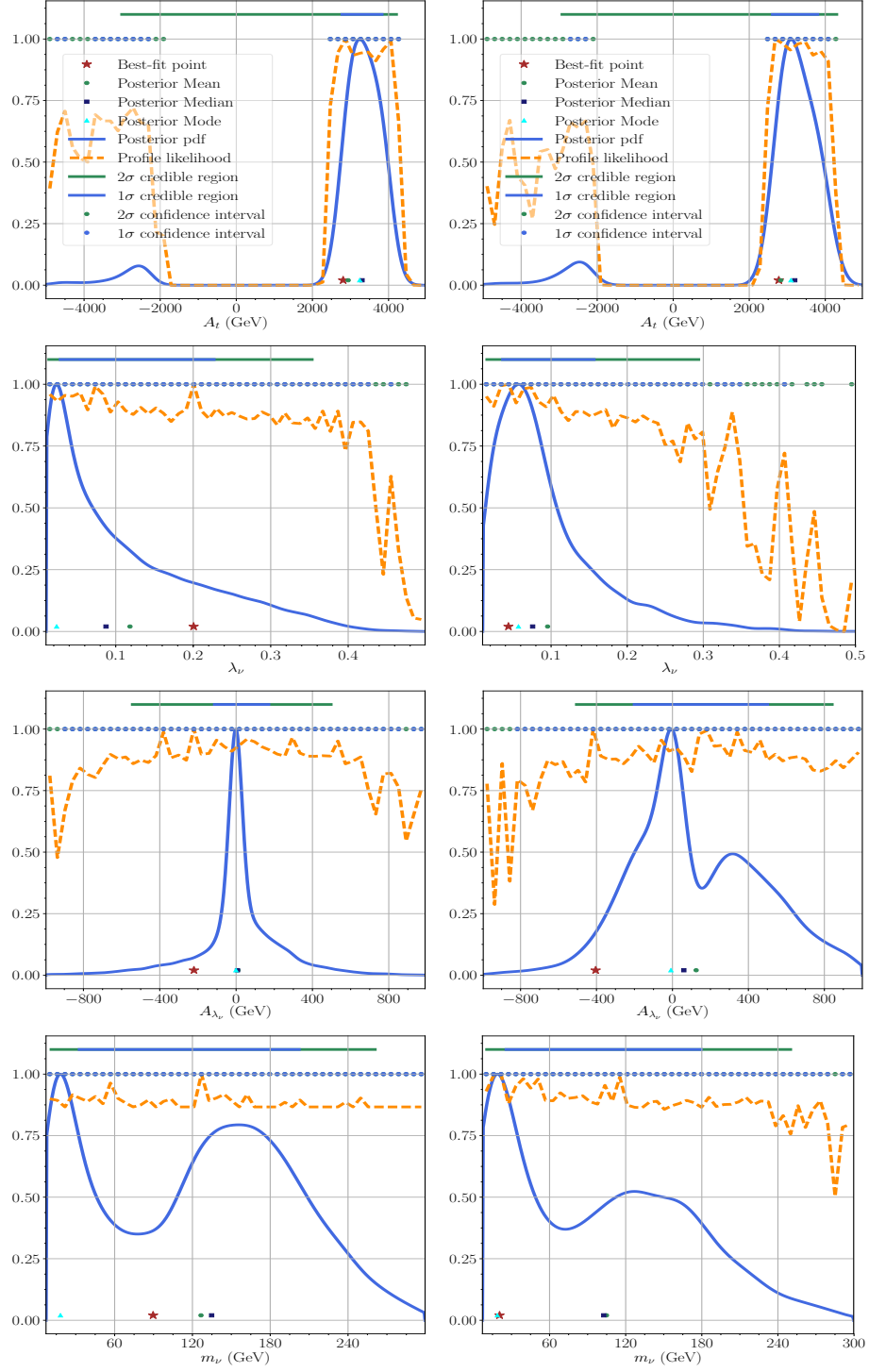


**Figure 2.** Same as Fig.1, but show the dependencies of the PDFs and PLs on  $A_t$ ,  $\lambda_\nu$ ,  $A_{\lambda_\nu}$  and  $m_\nu$  respectively.

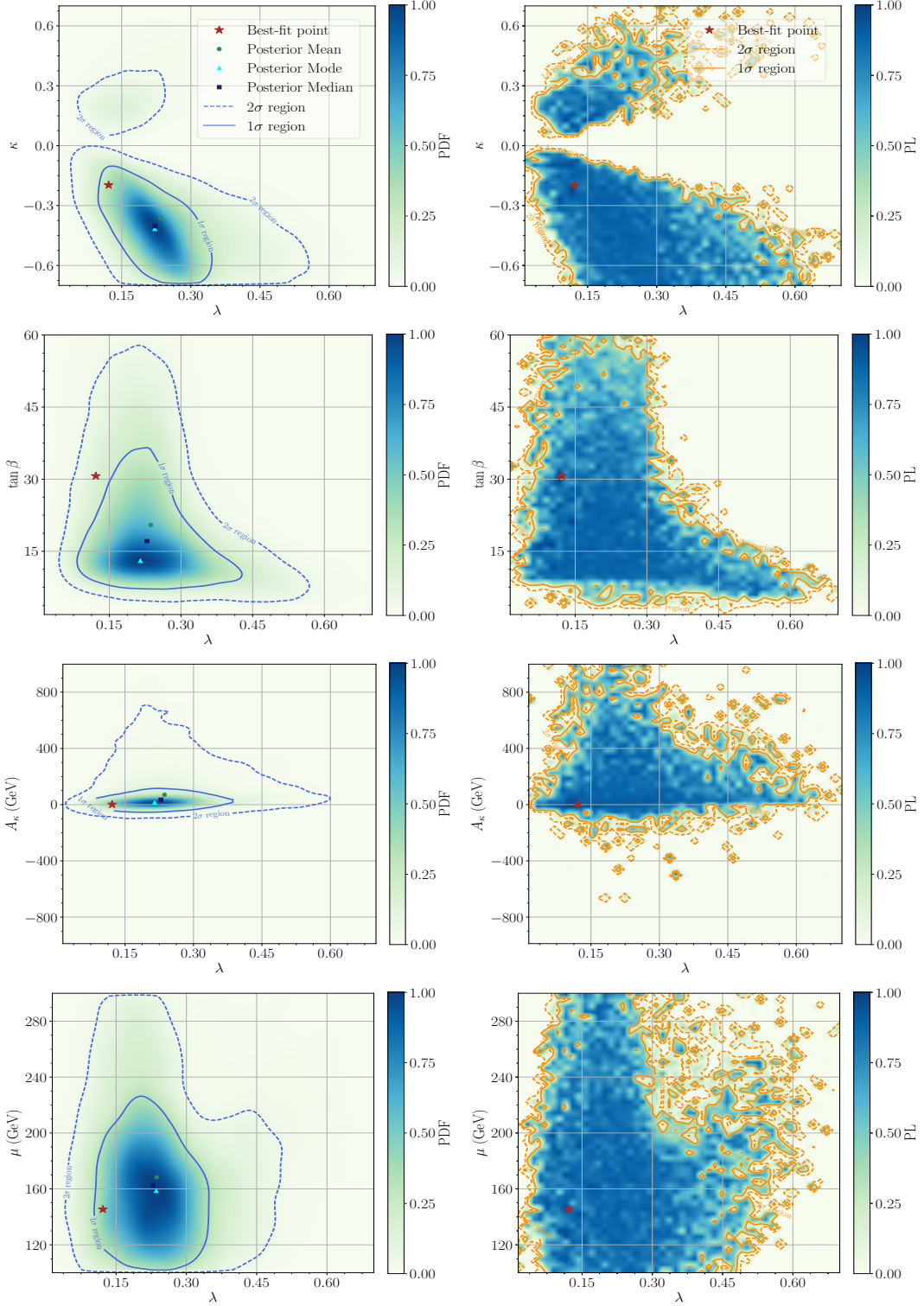


**Figure 3.** **Left panels:** Two-dimensional marginal posterior PDFs obtained from the parameter scan, which are projected on  $\kappa - \lambda$ ,  $\tan \beta - \lambda$ ,  $A_\kappa - \lambda$  and  $\mu - \lambda$  planes, respectively.  $1\sigma$  and  $2\sigma$  credible regions together with posterior mean, median and mode are also shown. **Right panels:** Similar to the left panels, but for two dimensional profile likelihoods. The best fit point as well as  $1\sigma$  and  $2\sigma$  confidence intervals are also plotted.

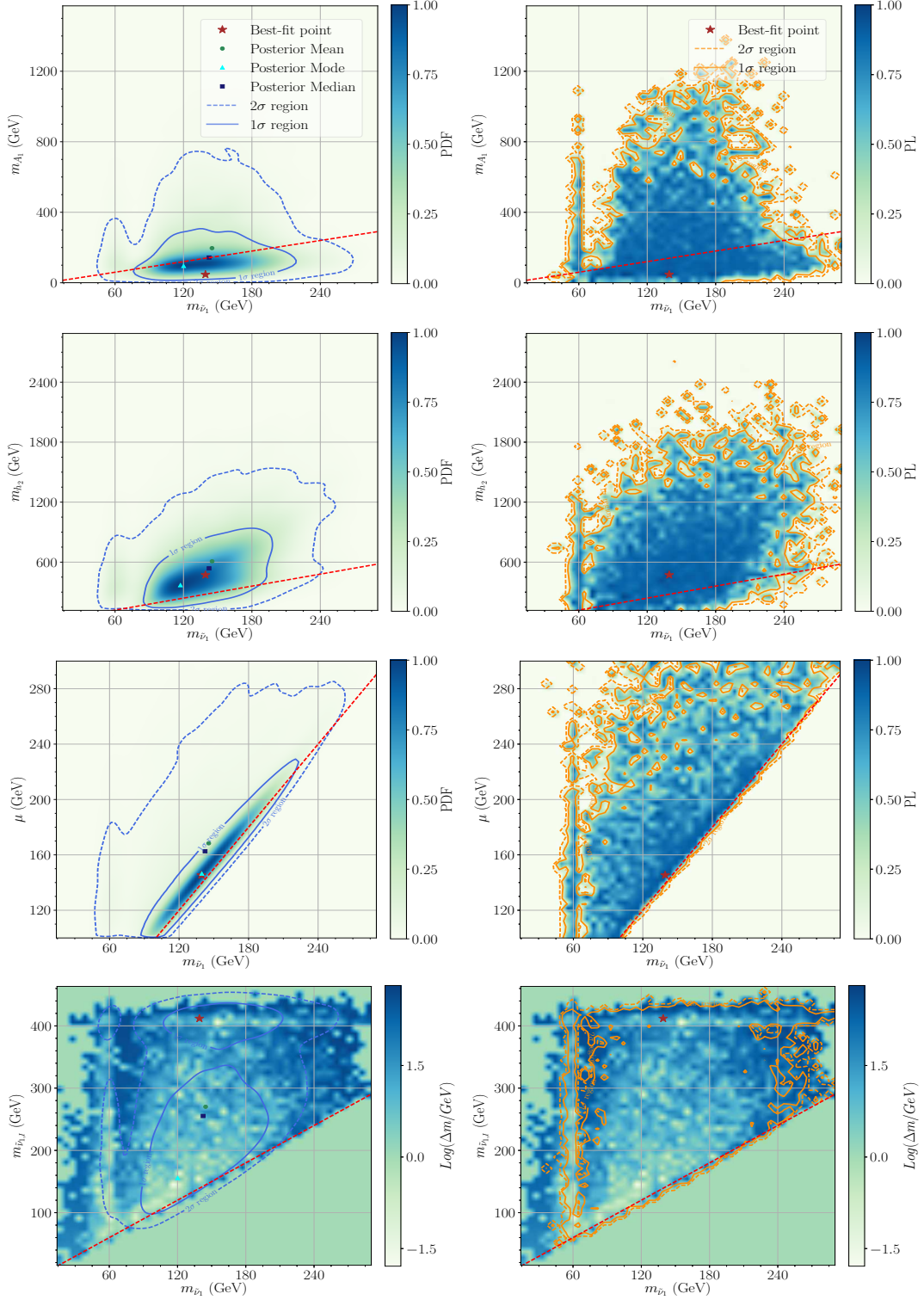


**Figure 4. Top three rows:** Similar to Fig.3, but projected on  $m_{A_1} - m_{\tilde{\nu}_1}$ ,  $m_{h_2} - m_{\tilde{\nu}_1}$  and  $\mu - m_{\tilde{\nu}_1}$  planes with the red dashed lines corresponding to the cases of  $m_{A_1} = m_{\tilde{\nu}_1}$ ,  $m_{h_2} = 2m_{\tilde{\nu}_1}$  and  $\mu = m_{\tilde{\nu}_1}$ , respectively. **Bottom row:** The distribution of the mass splitting  $\Delta m$  projected on  $m_{\tilde{\nu}_{1,I}} - m_{\tilde{\nu}_1}$  plane. Here  $\Delta m$  in each box on the plane (we have split the plane into  $70 \times 70$  equal boxes) is defined by  $\Delta m \equiv \min(|m_{A_1} - m_{\tilde{\nu}_1} - m_{\tilde{\nu}_{1,I}}|)$  for the samples allocated in the box. Different credible and confidence boundaries are also plotted for the left and right panel, respectively, with the red dashed lines corresponding to the case of  $m_{\tilde{\nu}_{1,I}} = m_{\tilde{\nu}_1}$ .

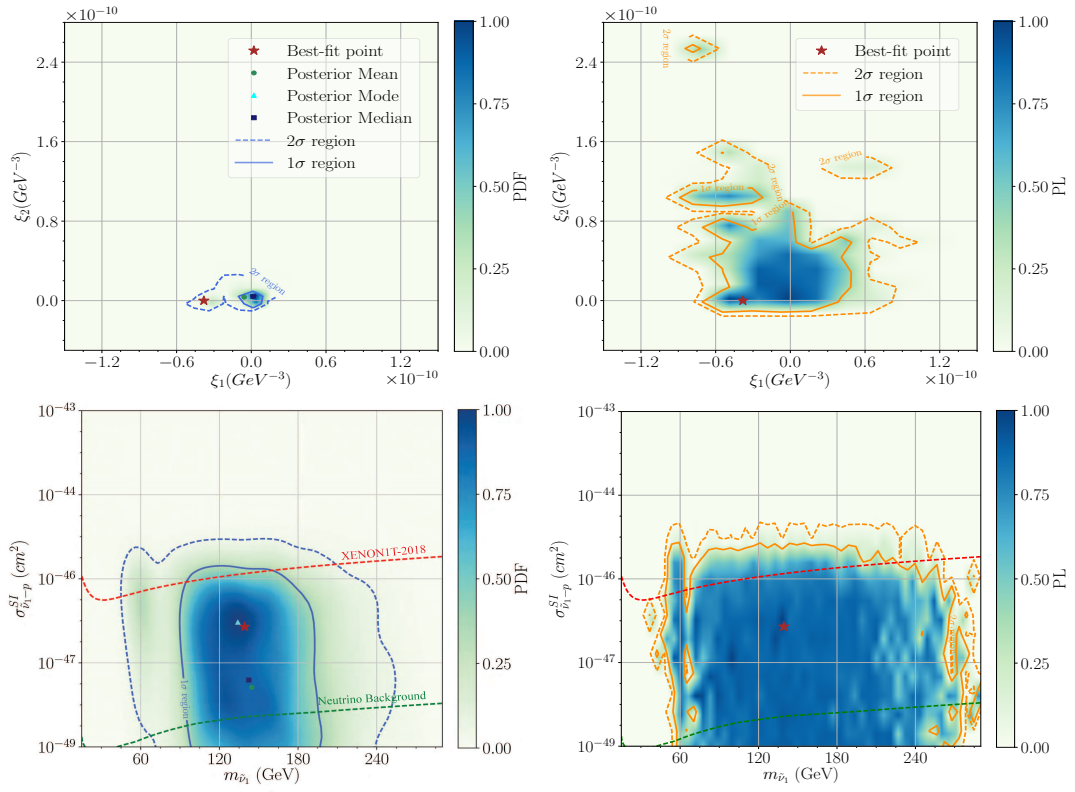


**Figure 5.** Similar to Fig.3, but projected on  $\xi_2 - \xi_1$  plane (top panel) and on  $\sigma_{\bar{\nu}_1-p}^{SI} - m_{\bar{\nu}_1}$  plane (bottom panel).

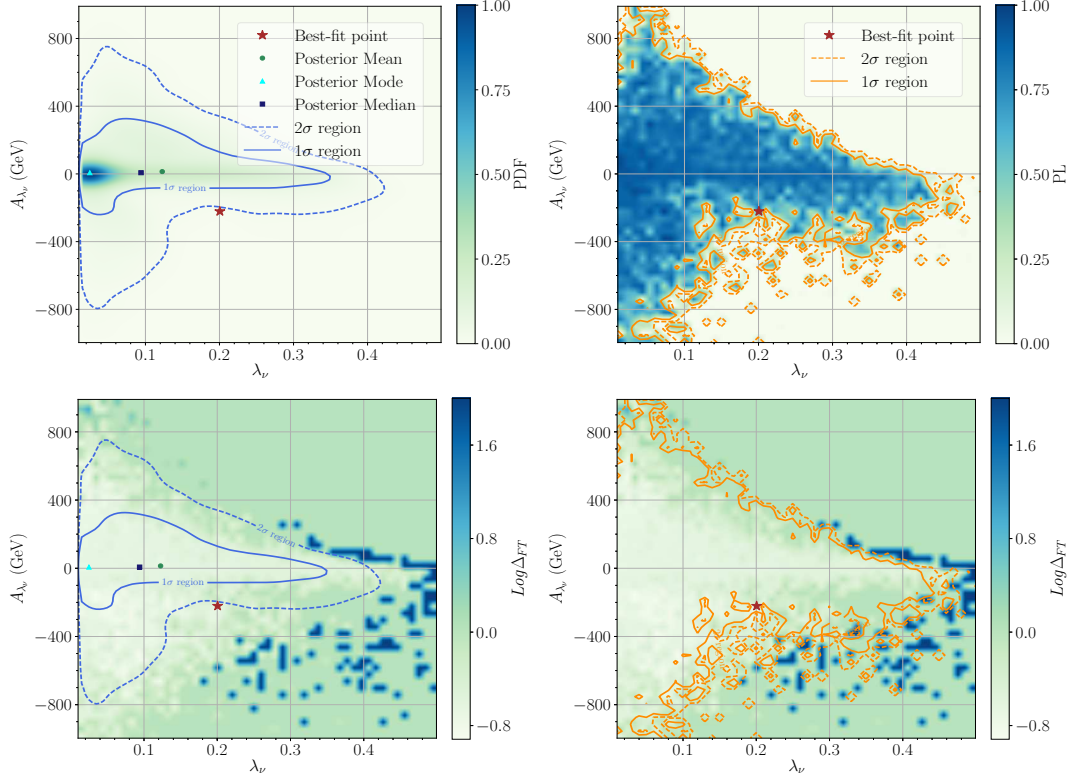


**Figure 6.** **Upper row:** Similar to Fig.3, but projected on  $A_{\lambda_\nu} - \lambda_\nu$  plane. **Lower row:** The minimum value of the fine tuning  $\Delta_{FT}$  required to satisfy the 90% upper bound of the XENON1T-2018 experiment on DM-nucleon scattering rate, which are projected on  $A_{\lambda_\nu} - \lambda_\nu$  plane. For each box on the parameter plane, the minimum value of  $\Delta_{FT}$  is obtained from the samples of the scan in following way: we only consider the samples in the box that satisfy the constraints of the XENON1T-2018 experiment, and pick out the minimum prediction of  $\Delta_{FT}$ .

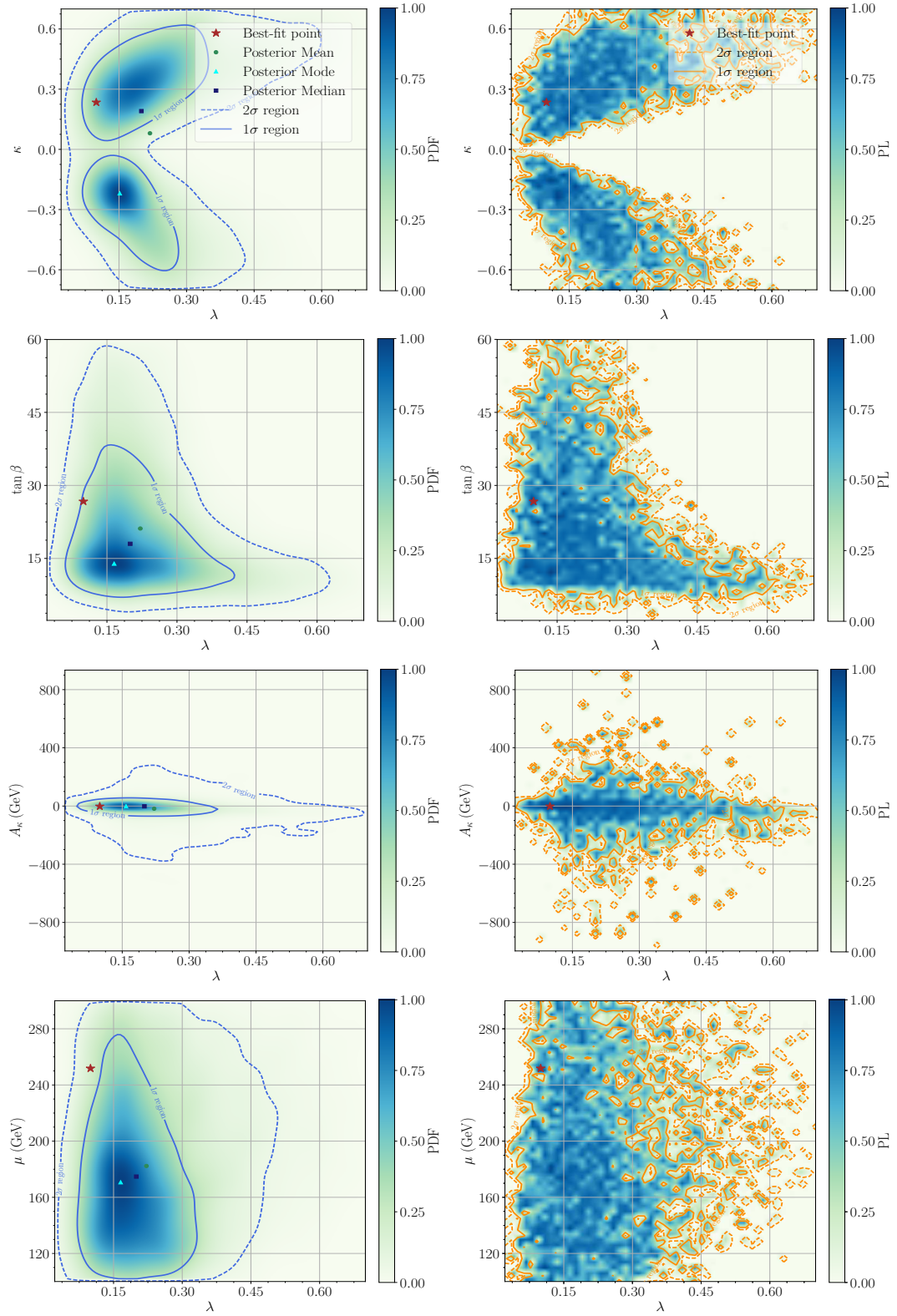


Figure 7. Similar to Fig.3, but for the case that the DM candidate  $\tilde{\nu}_1$  is CP-odd.

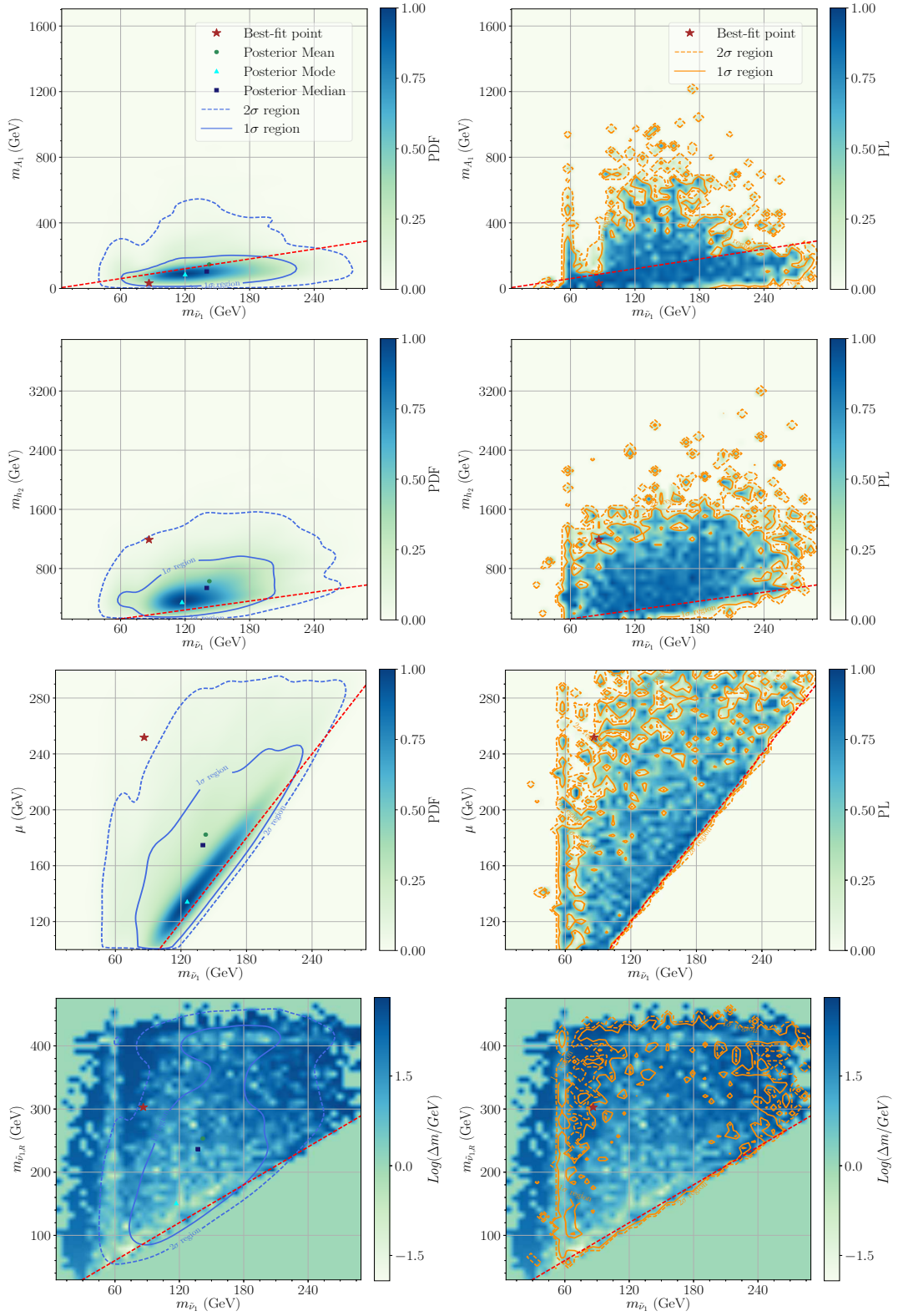
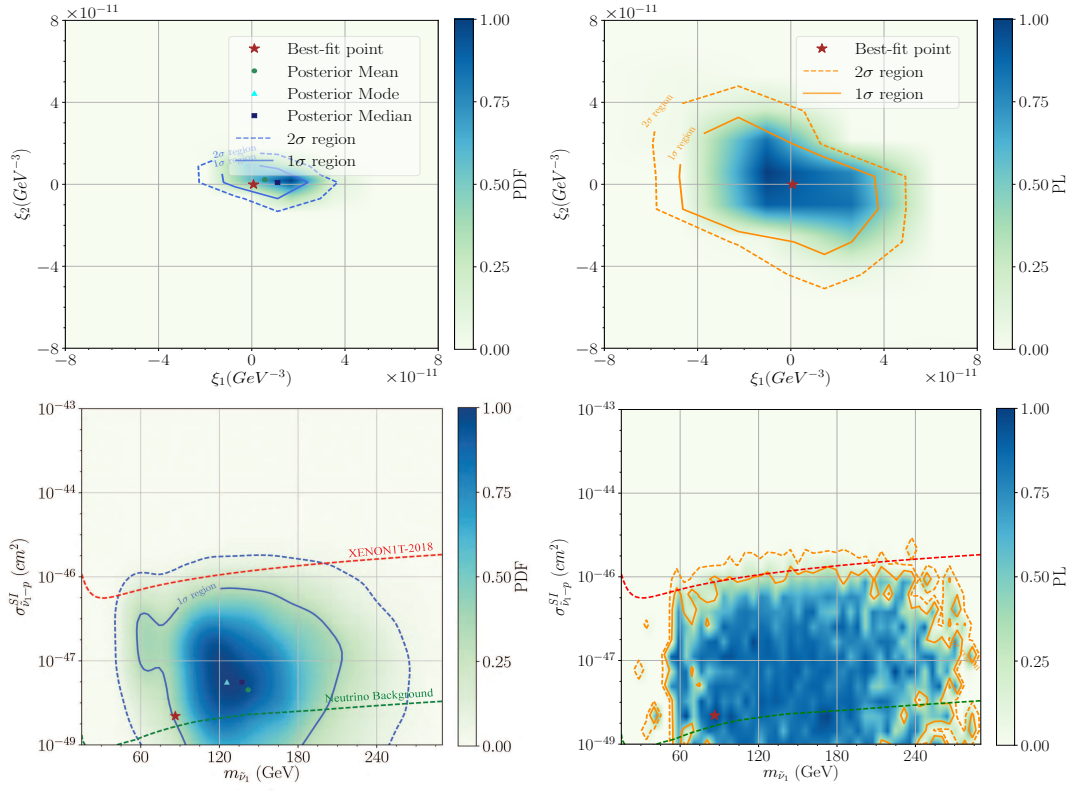
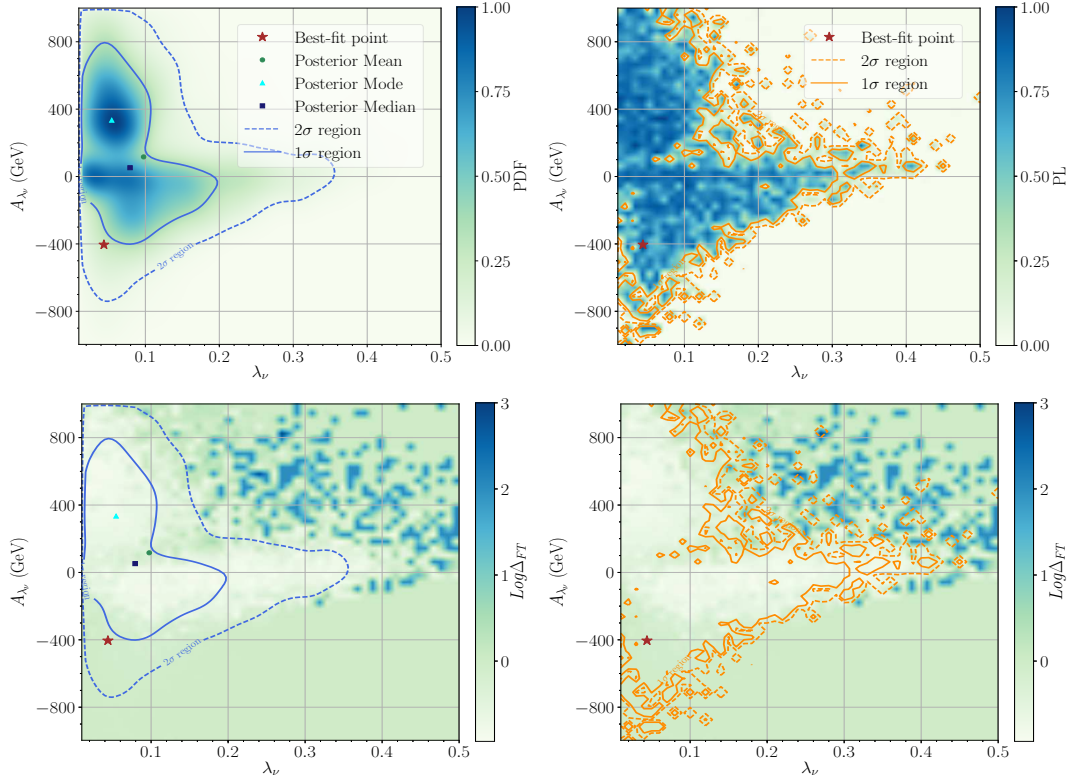


Figure 8. Similar to Fig.4, but for the case that the DM candidate  $\tilde{\nu}_1$  is CP-odd.



**Figure 9.** Similar to Fig.5, but for the case that the DM candidate  $\tilde{\nu}_1$  is CP-odd.



**Figure 10.** Similar to Fig.6, but for the case that the DM candidate  $\tilde{\nu}_1$  is CP-odd.

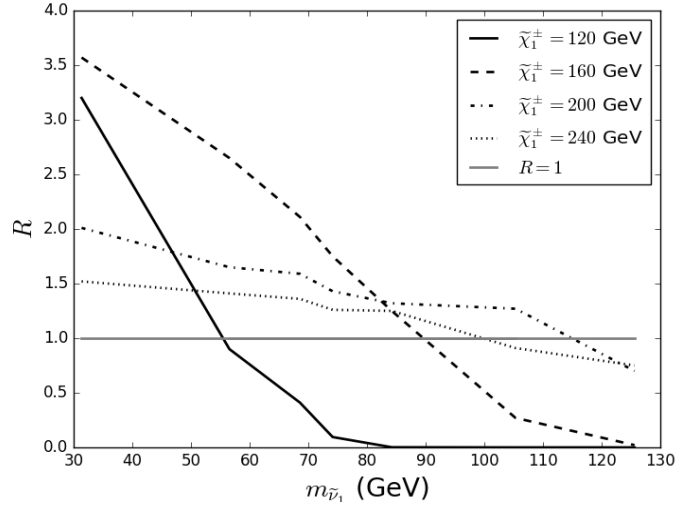


**Figure 11.** The dependence of  $R \equiv S/S_{95}^{OBS}$  for the analysis of the  $2\tau + E_T^{miss}$  signal at 8 TeV-LHC on the sneutrino DM mass. In the Type-I seesaw extension of the NMSSM, this signal comes from the process  $pp \rightarrow \tilde{\chi}_1^\pm \tilde{\chi}_1^\mp$  and we have fixed  $m_{\tilde{\chi}^\pm} = 120\text{GeV}, 160\text{GeV}, 200\text{GeV}, 240\text{GeV}$  in this figure. The cross sections of the process are calculated at next-to-leading order by the code Prospino[106]. In getting this figure, we have assumed  $Br(\tilde{\chi}_1^\pm \rightarrow \tilde{\nu}_1 \tau) = 100\%$ . If this is not satisfied, the  $R$  should be rescaled by the factor  $Br^2(\tilde{\chi}_1^\pm \rightarrow \tilde{\nu}_1 \tau)$ .